New photonic carbon nanostructures

PhD Thesis

Author:	mgr inż. Patrycja Taborowska
Supervisor:	prof. dr hab. inż. Dawid Janas
Co-supervisor:	dr inż. Andrzej Dzienia

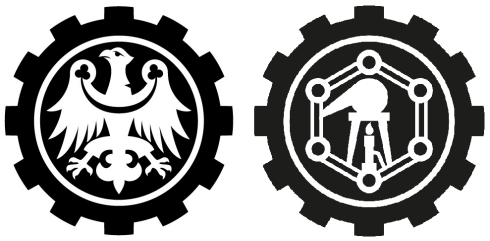

Faculty od Chemistry
Silesian University of Technology
Gliwice, Poland

2026

Abstract

The unique optical properties of chirality-sorted single-walled carbon nanotubes (SWCNTs) make them attractive candidates for modern photonic applications. However, their photoluminescent (PL) emission must first be harnessed through careful chemical modification, *i.e.*, covalent attachment of functional groups to their surface. Sorted SWCNT dispersions are prepared either in water with the aid of surfactants or in organic solvents with the aid of conjugated polymers, depending on the intended application. Water-based systems for SWCNT sorting and functionalization are well described in the literature, in contrast to organic-based systems, although in both cases the reaction mechanisms remain unclear.

In this work, improved conditions of chiral sorting of the commercially available SWCNTs using conjugated polyfluorenes in toluene were described. The improvements not only lead to substantial increase of quality and quantity of the close-to monochiral (6,5) and (7,5) SWCNT dispersions, but also allowed to reduce the consumption of the raw SWCNT material and the polymer, as well as time and energy. This was obtained by repeated extraction of the desired SWCNTs in a closed-loop process, allowing to re-cycle the source of nanotubes, polymer and solvent. Then, the high-quality chirally-uniform dispersions in organic solvents were functionalized using radicals originating from decomposition of benzoyl peroxide (BPO). Proper selection of the reactant concentration, temperature and type of solvent allowed to activate one or radical decay pathways, *i.e.* spontaneous or both induced decomposition. The obtained radicals attack the SWCNTs, grafting them with functional groups via C-O or C-C bonds, both leading to distinct emission features in the PL spectra of the SWCNTs. Further, it was shown, that the symmetrically substituted derivatives of BPO create a toolbox for quick and effective attachment of the functional groups to the surface of SWCNTs, allowing control over the attached groups density and light emission wavelength. Notably, the electron-deficient reactants were found the most effective, which corroborated previous finding and allowed for better understanding of the reaction mechanism. Importantly, the presented method was also successfully used to functionalize larger SWCNTs than the (6,5), even though their reactivity is significantly lower.

Keywords: *single-walled carbon nanotubes, conjugated polymers, aryl peroxides, selective extraction, functionalization, photoluminescence*

Streszczenie

Unikalne właściwości optyczne chiralnie jednorodnych jednościennych nanorurek węglowych (ang. *Single-Walled Carbon Nanotubes* – SWCNTs) stanowią o ich ogromnym potencjale do zastosowań w nowoczesnej fotonice. Zachodzi jednak potrzeba modyfikacji ich właściwości fotoluminescencyjnych (ang. *Photoluminescence* – PL) poprzez staranną modyfikację chemiczną, w tym przypadku polegającą na kowalencyjnym przyłączeniu grup funkcyjnych na ich powierzchni. Chiralnie jednorodne dyspersje SWCNT przygotowywane są w środowisku wodnym albo w rozpuszczalnikach organicznych, w zależności od przyszłego zastosowania. Systemy oparte na środowisku wodnym są dobrze znane w literaturze, w przeciwieństwie do systemów organicznych, jednak w obydwu przypadkach mechanizm funkcjonalizacji SWCNT nadal pozostaje niewyjaśniony.

W niniejszej pracy najpierw poprawiono warunki sortowania komercyjnie dostępnych SWCNT za pomocą polimerów skoniugowanych w rozpuszczalnikach organicznych. Wprowadzone modyfikacje procesu wpłynęły na podniesienie jakości i wydajności uzyskania dyspersji (6,5) oraz (7,5) SWCNT, pozwoliły ograniczyć zużycie surowego materiału SWCNT oraz polimerów, a także czasu i energii, dzięki opracowaniu zamkniętego procesu umożliwiającego odzyskanie zarówno nanorurek, polimeru jak i rozpuszczalnika. Wysokiej jakości dyspersje chiralnie jednorodnych SWCNT w rozpuszczalnikach organicznych zostały następnie sfunkcjonalizowane za pomocą rodników pochodzących z rozpadu nadtlenku benzoilu (BPO). Właściwy dobór stężenia reagentów, temperatury i rodzaju rozpuszczalnika pozwalał aktywować jeden lub oba mechanizmy rozpadu rodników, tj. rozpad spontaniczny lub indukowany. Uzyskane rodniki atakowały SWCNT, tworząc wiązania kowalencyjne typu C–O lub C–C, prowadzące do emisji na różnych długościach fali w widmie PL nanorurek. Ponadto wykazano, że symetrycznie podstawione pochodne BPO stanowią zestaw narzędzi do szybkiej i wydajnej funkcjonalizacji SWCNT, pozwalając kontrolować gęstość upakowania grup funkcyjnych na ich powierzchni i długość fali emisji. Co istotne, najbardziej efektywne były reagenty ubogie w elektrony, co potwierdziło wcześniejsze obserwacje i umożliwiło lepsze zrozumienie mechanizmu reakcji. Ponadto, przedstawiona metoda została skutecznie wykorzystana do funkcjonalizacji SWCNT o większych średnicach niż w przypadku najbardziej popularnej chiralności (6,5), pomimo ich niższej reaktywności.

Słowa kluczowe: *jednościenne nanorurki węglowe, polimery sprzężone, nadtlenki, selektywna ekstrakcja, funkcjonalizacja, fotoluminescencja*

Acknowledgments

Over four year long research, summarized in this thesis, was an amazing scientific adventure for the author. It would not be possible without certain people, their knowledge, enthusiasm, and patience shown everyday in laboratory, office, class or at home.

First of all I would like to thank my supervisors, Prof. Dawid Janas and Dr Andrzej Dzienia, as well as my collaborators and colleagues from the FNano team, especially Dr Błażej Podleśny, Dr Tomasz Wasiak, Dominik Just, Łukasz Czapura, Jakub Ćwiertnia, Paweł Kubica-Cypek, but also all the other PhD and younger students working with us. It was a pleasure to every day discover a fascinating world of carbon nanotubes together and I am sure that I have learned a lot from each of you.

Special thanks for Dr Anna Korytkowska-Wałach who was my guide when it came to teaching classes and I will always be inspired by her kindness.

Last but not least, I would like to thank Karolina Juszczak, Ravikant Adalati, Igor Kulik and Michał Kolany for the emotional support and honest critical opinions from different points of view, whenever I needed them.

The author would also like to thank the National Science Centre, Poland (under the SONATA program, Grant agreement UMO-2020/39/D/ST5/00285) for funding this research.

Contents

List of publications

The presented dissertation consists of the following collection of published and thematically related articles, and one patent:

P1 P. Taborowska, A. Mielanczyk, A. Dzienia and D. Janas, **Environmentally conscious highly effective sorting of single-walled carbon nanotubes using recurrent conjugated polymer extraction.**, *ACS Sustainable Chem. Eng.*, 13:621–636, 2025. DOI: 10.1021/acssuschemeng.4c08836.

P2 P. Taborowska*, A. Dzienia* and D. Janas, **Unraveling aryl peroxide chemistry to enrich optical properties of single-walled carbon nanotubes.**, *Chem. Sci.*, 16:374–1389, 2025. DOI: 10.1039/d4sc04785k.

P3 A. Dzienia*, P. Taborowska*, P. Kubica-Cypek and D. Janas, **Programing optical properties of single-walled carbon nanotubes with benzoyl peroxide derivatives of tailored chemical characteristics.**, *Mater. Horiz.*, 12:9040–9056, 2025. DOI: 10.1039/D5MH01129A.

* Both authors contributed equally.

	P1	**P2**	**P3**	**sum**
IF	7.3	7.4	10.7	25.4
MNiSW points	140	140	200	480

Pat1 A. Dzienia, D. Janas, P. Taborowska, D. Just: Method of selective isolation of semi-conducting single-walled carbon nanotubes (Sposób selektywnej izolacji półprzewodnikowych jednościennych nanorurek węglowych), Polish Patent: Pat.248351, 2025.

Abbreviations

BPO	Benzoyl Peroxide
CNT	Carbon Nanotube
CP	Conjugated Polymer
CPE	Conjugated Polymer Extraction
CoMoCAT	Cobalt-Molybdenum Catalyst
CVD	Chemical Vapor Deposition
DOS	Density of States
F8BT	poly(9,9-dioctylfluorene-*alt*-benzothiadiazole)
NIR	Near Infrared
NMR	Nuclear Magnetic Resonance
PFO	poly(9,9-dioctylfluorenyl-2,7-diyl)
PFO-BPy6,6'	poly(9,9-dioctylfluorene-*alt*-6,6'-bipyridine)
PL	Photoluminescence
SEC	Size Exclusion Chromatography
s-SWCNT	semiconducting Single Walled Carbon Nanotube
SWCNT	Single Walled Carbon Nanotube
THF	Tetrahydrofuran
QY	Quantum Yield

1. Introduction

1.1. Electrical and optical properties of single-walled carbon nanotubes (SWCNTs)

Nanotechnology as a concept of manipulation of nanometer-size objects, was introduced to a broader audience by Richard P. Feynman in his seminal lecture delivered at Caltech in 1959.[1] The existence of graphene and certain fullerenes had already been postulated, although their experimental verification came decades later. In contrast, carbon nanotubes (CNTs) were observed earlier, in 1952, by Radushkevich and Lukyanovich,[2] then during the 1970s by Endo *et al.*[3] and other research groups, reporting the existence of hollow carbon filaments with nanometer-scale diameters. Their precise structure remained unclear until two decades later, when Ijima for the first time presented the detailed architecture of graphene-based tubes and described a method for their synthesis.[4] Following this discovery, the researchers worldwide have experimentally demonstrated that different CNT types exists and each of them exhibits slightly distinct sets of properties, underscoring their exceptional potential in nanoelectronics, nanobiotechnology, nanophotonics, and nanomechanics.

SWCNT consists of one graphene layer. Analogically, multi-walled CNT (MWCNT) is composed of two or more graphene layers, which makes properties of these structures much more complicated to describe. CNTs usually have 0.5–2 nm in diameter and several micrometers in length, so their aspect ratio can exceed 10 000, making them the most anisotropic material ever produced. They are sometimes regarded as 1D conductors. As bulk material, they can be easily fixed in the form of thin films or threads, which are lighter and more elastic than metals and on the other hand, they perform better than conductive polymers. Initially, the CNTs were appreciated for their electrical[5–7] and thermal conductivity,[8,9] as well as mechanical performance.[10,11] However, their real potential lies in the astonishing mathematically described diversity, originating from the observation, that the hexagonal lattice of carbon atoms (graphene) that forms a tube, can be oriented in many different directions (Figure 1.1a). The implications of this simple fact are certainly interesting.

To define the particular type, known as "chirality" of the SWCNT, a vector can be drawn around its circumference. It is called a chiral vector C_h. Upon imaginary unrolling of the graphene sheet, C_h can be conveniently decomposed into unit vectors a_1 and a_2 (red and blue

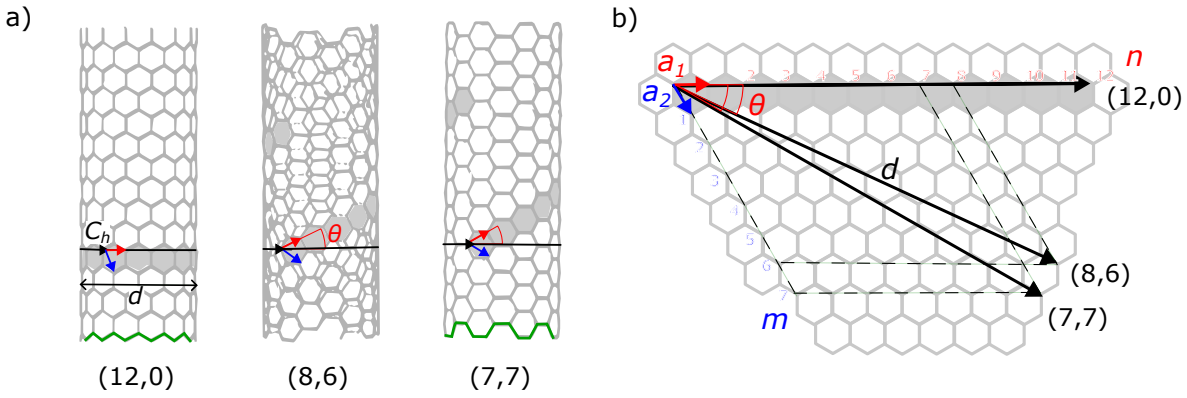

Figure 1.1. Structure of SWCNT. a) SWCNTs of three different chiralities (n, m) are presented, with chiral vectors C_h and chiral angles θ. b) Decomposition of C_h to unit vectors a_1 and a_2.

in Figure 1.1) with indices n and m. The SWCNT is termed as of (n, m) chirality. Knowing the indices, the values of the chiral angle θ and diameter d can be calculated:

$$C_h = na_1 + ma_2$$

$$d = \frac{a}{\pi}\sqrt{n^2 + nm + m^2}$$

$$\theta = \arctan\left(\frac{\sqrt{3}m}{2n + m}\right)$$

where $a = 0.246$ nm is a graphene lattice constant.

The majority of the properties of the nanotube depend on the chiral vector, most notably, if $n - m$ is a multiple of 3, the SWCNT is most probably metallic or semi-metallic, *e.g.* $(12, 0)$ and $(7, 7)$ SWCNTs shown in Figure 1.1. Others, *e.g.* $(8, 6)$, are moderately semiconducting, with bandgap depending on the chirality (diameter).[12] Those rules do not apply to very small-diameter SWCNTs, due to their significant surface curvature. Additionally, due to their specific symmetry, the (n, n) SWCNTs are often referred to as 'armchair', and $(n, 0)$ SWCNTs – as 'zig–zag', because the pattern created by the carbon atoms laying on the circumference (depicted with green lines in Figure 1.1a). Other species are 'chiral' SWCNTs.

To understand a little better, why the SWCNTs exhibit such impressive mechanical and electrical performance, we will now focus on a single carbon atom in their structure. Electron configuration of a C atom in a ground state is $1s^2$, $2s^2$, $2p^4$, however, in the graphene plane it is connected to other C atoms via a sp^2 planar bond, comprising of three σ bonds, formed from the hybridization of the $2s$, $2p_x$ and $2p_y$ orbitals (Figure 1.2a). The remaining $2p_z$ orbital, perpendicular to the graphene plane, overlaps with the other $2p_z$ orbitals of the neighboring C atoms, and together they form a system of covalent π bonds (Figure 1.2b). Importantly, different orbitals have different corresponding energies – the lower energy σ orbitals form a valence

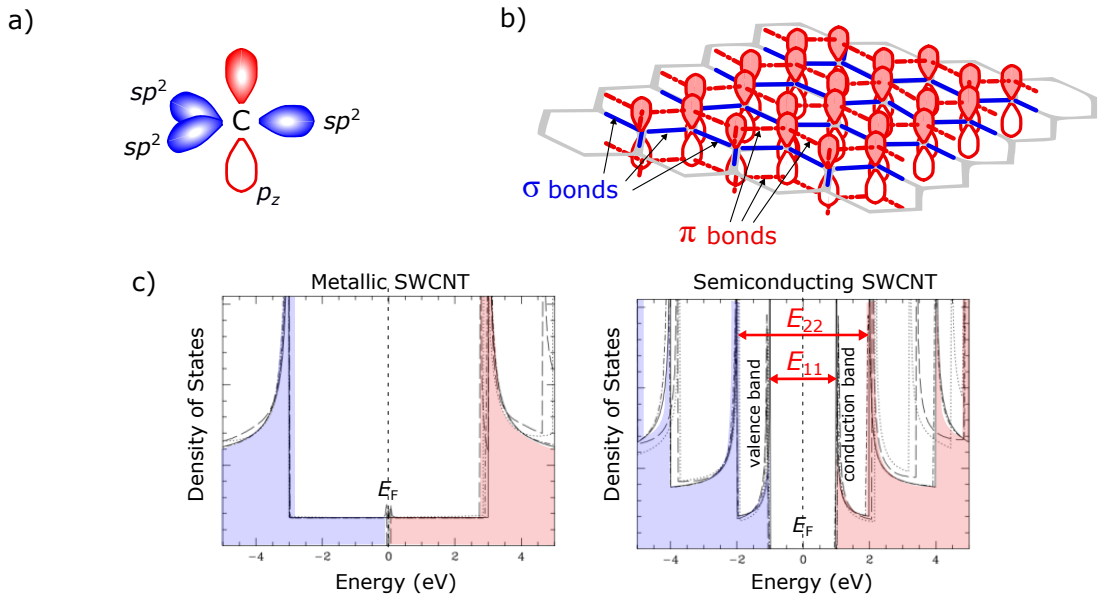

Figure 1.2. a) Representation of the sp^2 hybridization of a single carbon atom in a graphene structure. b) The system of σ and π bonds on the surface of SWCNT. c) DOS of metallic and semiconducting SWCNT,[13] with sharp van Hove singularities, Fermi energy level located at 0 eV, and representation of E_{11} and E_{22} interband transitions. This transitions can be observed in optical spectra of the SWCNTs of mainly one chirality.

electron band, and the higher energy π orbitals form a conduction band, which significantly influences charge transport and mechanical strength of the nanotubes. The system of π-bonds is also responsible for the van der Waals forces between the CNTs, which make them susceptible to agglomeration. Fortunately, it is possible to properly separate the SWCNTs from each other, which will be discussed later, and release the unique set of properties carried by each chirality type.

Throughout the 1990s, the structure of SWCNT was defined in terms of their helical and rotational symmetries.[14] This knowledge was used for establishing a universal relationship for DOS (Density of States) near the Fermi level (E_F). It consists of sharp van Hove maxima at energies dependent on nanotube chirality (Figure 1.2c), which are the characteristic signature of the strongly one-dimensional nature of electrical conduction.[13] It was found that when $n - m$ is a multiple of 3, the symmetry in the arrangement of π bonds leads to the finite value of carriers in DOS near the Fermi level, which as a consequence makes SWCNTs metallic. On the other hand, lack of this symmetry results in an energy gap around the Fermi level, and semiconducting behavior of SWCNTs. The bandgap in semiconducting SWCNT (s-SWCNT) was found to be inversely proportional to its diameter.[15] In the next decade it was discovered that, in addition to describing the electrical conductivity in SWCNTs, the DOS also helps comprehending their optical behavior. The optical absorption spectrum of semiconducting nanotubes is dominated by a series of sharp interband transitions, at energies denoted E_{11}, E_{22}, E_{33} etc., associated

with the van Hove singularities.[16] The exact positions of the peaks depend on the chirality. Optical excitation of the SWCNT in their second van Hove transition E_{22}, is followed by photoluminescent (PL) emission in the first transition E_{11}. Nanotubes available in commercial distribution emit in NIR region, specifically 800–1600 nm range. These findings opened the road to applications of the SWCNTs as a set of precisely tuned optical tools for photonics, from bioimaging to telecommunication.[17]

Soon, this road split into two, as it was observed that the PL intensity from SWCNTs is unsatisfactory. PL quantum yield (QY) *i.e.* rarely exceeds 1% for non-modified SWCNTs in dispersion.[18] In pristine nanotubes, most of possible paths of relaxation lead to non-radiative recombination, when the excitons are quenched on the nanotube ends or hexagonal structure imperfections. Soon, the methods of functionalization, meaning improving the PLQY through careful chemical modification, were developed simultaneously with the methods of sorting of the SWCNTs according to chirality. Both those aspects are of great importance for obtaining selective PL emission spectra, necessary for most demanding applications. Functionalization and chiral isolation are usually separate processes. Sometimes, the mixture of chiral species is first modified with certain functional groups, and then one of the chiralities is extracted; other procedures rely on isolating the particular chirality and modifying it afterwards. The next sections of this work are dedicated to showing these two processes in greater detail.

1.2. Sorting SWCNTs by chirality type

SWCNTs can be produced using various methods, the most common being catalytic chemical vapor deposition (CVD).[19–21] Less frequently employed techniques include laser ablation,[22] plasma torch,[23] and arc discharge.[24] However, regardless of the synthesis method used, the resulting material is typically a mixture of many different chiralities. At the start of the 21st century, significant advances were made in producing enriched mixtures of SWCNTs.[25–27] These enriched materials feature a limited range of chiral species. For example, CoMoCAT SG65i contains *c.a.* 15 chiralities with diameters ranging from 0.7–0.9 nm. Moreover, this material composed in >90% of SWCNTs, demonstrates a notable chirality bias, with approximately 40% of them exhibiting the (6,5) chirality. This selective enrichment was achieved through carbon deposition on a $CoMo/SiO_2$ catalyst to CVD process.[26] Using high-pressure, carbon monoxide and in situ generated iron catalysts (HiPco), produces slightly bigger SWCNTs (0.8–1.2 nm in diameter) which have carbon purity of about 80%.[25] Further, Tuball SWCNTs with diameters from 1 to 2 nm are obtained using special catalysts.[27] Despite these advancements, achieving high chiral purity remains a significant challenge for optical and electrical applications. *E.g.* for photonic sensors and emitters, isolating SWCNTs of single chirality is crucial, due to different absorption and emission wavelengths of each SWCNT species. This demands have spurred the development of post-synthesis techniques

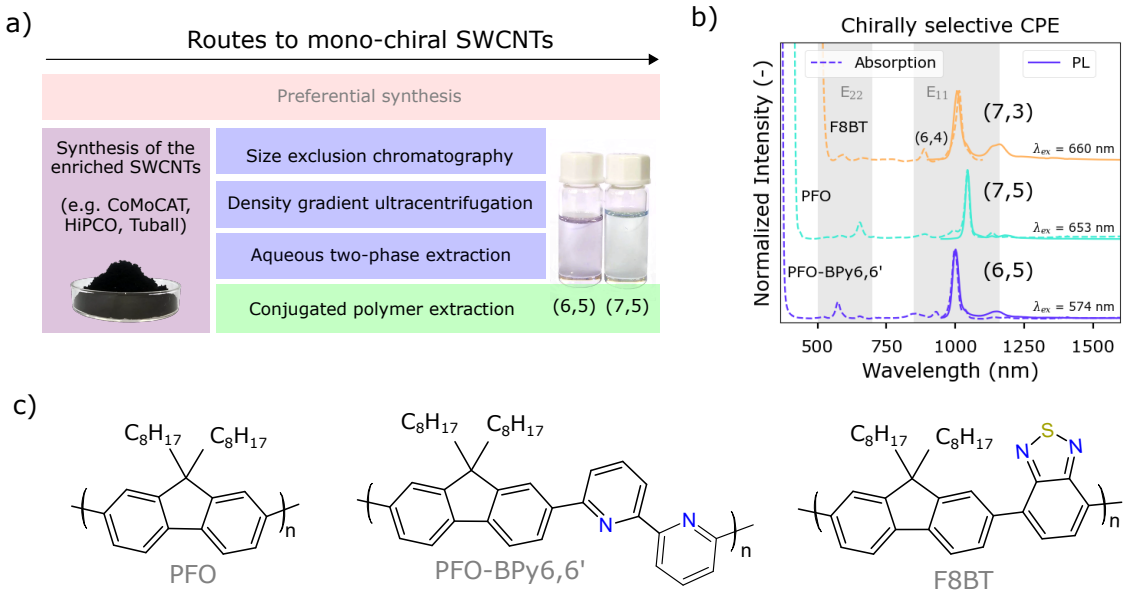

Figure 1.3. a) Selected methods of obtaining close-to monochiral SWCNTs, according to the reference.[28] b) Optical spectra (absorption and PL emission) of the close-to monochiral SWCNTs extracted by the conjugated polyfluorenes PFO, PFO-BPy6,6' and F8BT (visible on the left side of absorption spectra), in organic solvents. The wavelength ranges of optical bands E_{11} and E_{22} were shaded gray. c) Structures of the fluorene-based chirally selective CPs, used to obtain spectra from (b).

for sorting the synthesized SWCNTs by chirality. Currently, the most effective approach for obtaining monochiral SWCNTs involves synthesizing chirally enriched materials followed by chirality-specific sorting (Figure 1.3a).[28]

As it was mentioned earlier, carbon nanotubes are highly susceptible to aggregation due to the van der Waals forces, and a consequence, deterioration of the electrical and optical properties is observed for macroscopic CNT structures. Isolation of the nanotubes from each other is then necessary to preserve the desired properties of the SWCNTs. Moreover, in the raw material, in addition to different SWCNTs, there are also impurities such as other fullerenes, catalysts, or amorphous carbon. The chiral sorting and isolating the SWCNTs from each other are conducted in one process with removing these impurities. Usually, as-synthesized SWCNTs are dispersed in an aqueous solution with the aid of surfactants, such as sodium dodecyl sulphate[29] or sodium dodecylbenzene sulphonate.[30] The dispersions can be effectively divided into two or more fractions by several methods: size exclusion column chromatography (SEC),[31] density gradient ultracentrifugation (DGU)[32] or aqueous two-phase extraction (ATPE).[33] SEC allows to produce multiple fractions of high chiral purity in one operation, but on the other side, the technique is complicated, non-scalable and requires expensive equipment. Similar problems were encountered with DGU. On the other hand, ATPE is used for efficient and much more affordable separation of just one chirality (or conductivity type, depending on the system of surfactants) from the others.

In 2007, yet another approach was proposed. Instead of water and surfactants, organic solvent and specific conjugated polymers (CPs) were used to stabilize the dispersion of SWCNTs.[34,35] Similarly to ATPE, the extraction process is simple to conduct and requires only standard laboratory equipment. First, the initial enriched mix of SWCNTs is sonicated with the CP in the solvent. During sonication, the polymer selectively wraps and disperses a subset of nanotubes. In the second step, bundles of non-dispersed nanotubes and impurities are removed by mild centrifugation. After centrifugation, the supernatant contains only selected SWCNTs wrapped with conjugated polymer, dispersed in organic solvent. Absorption and PL emission spectra allow to confirm the presence of only one chiral species in CP-extracted SWCNT dispersions (Figure 1.3b), assuring signal selectivity. High volatility of the dispersions in organic solvents enables facile deposition of the thin nanotube films on various substrates, which is convenient for modern electronics.

Despite the described simplicity of the CPE (CP extraction) process, the exact mechanism of polymer selection remains unclear. Depending on the polymer structure, kind of solvent, initial composition of the SWCNT mixture and the parameters of sonication and centrifugation, it is possible to obtain highly enriched s-SWCNTs (purity >99%),[36,37] close-to monochiral SWCNTs,[29,38–40] or even SWCNTs of selected chirality in only one enantiomeric form.[41] Here, the discussion will focus on methods for sorting SWCNTs by chirality type, although it must be said that our understanding of the process was inherited from earlier conducted research on sorting by conductivity type, *i.e.* extraction of s-SWCNTs.[36,42,43] Due to the fact that optimal structure of the CPs and methods of their synthesis are separate, at least equally complicated and very recent issues, which make them out of scope of this work; only basic understanding of these processes, necessary for further discussion, was presented below.

Among many different structures of the CPs, most promising results were obtained with polymers based on the fluorene monomer unit. First, Nish *et al.* showed that poly(9,9-dioctylfluorenyl-2,7-diyl) (PFO, structures in Figure 1.3c) enables selective extraction of (7,5) chirality from (6,5)-enriched CoMoCAT SWCNTs.[44] The same polymer was used for extracting (10,9) SWCNTs from HiPco,[45] which underscores the importance of the composition of starting material. Ozawa *et al.* introduced the bipyridine (BPy) moiety into the PFO, creating PFO-BPy6,6', which allowed for the selective extraction of (6,5) SWCNTs from (6,5)-enriched CoMoCAT material.[46] The (6,5) SWCNT wrapped with PFO-BPy6,6' soon was adapted as a model system, due to relatively high extraction efficiency, which enabled wide ranging experimental research. Another polymer, poly(9,9-dioctylfluorene-*alt*-benzothiadiazole) (F8BT) was used for the extraction of nanotubes such as (7,3), (9,4), (10,5).[40,47] Most efficient systems, which enabled significant enrichment or close-to monochiral extraction, were summarized in Table 1.1. Although these systems are commonly used in laboratory practice to produce the chirally selective SWCNT dispersions and films, the mechanism of polymer selection remains mostly unexplained. It was shown, that the CP affinity to the SWCNT type

Table 1.1. Known systems of close to monochiral extraction of SWCNTs using conjugated polymers.

Extracted Chirality	Source SWCNTs	Conjugated Polymer	Solvent	Ref.
(6,5)	CoMoCAT SG65i	PFO-BPy6,6'	toluene	[46]
(7,5)	CoMoCAT SG65i	PFO	toluene	[38,44]
(7,3)	CoMoCAT SG65i	F8BT	toluene-tetralin	[40]
(7,6)	CoMoCAT SG76	PFH-A[a]	toluene	[53]
(9,5)	CoMoCAT SG76	PFO-A[b]	toluene	[53]
(9,8)	from $CoSO_4$/SiC catalyst	PFH-A	toluene	[54]
(10,9)	RN-220 (plasma torch)	PFO	tetralin	[45]

[a] poly[9,9-dihexyfluorenyl-2,7-diyl-co-(9,10-anthracene)].
[b] poly[9,9-dioctyl-2,7-divinylfluorenylene-alt-co-(9,10-anthracene)].

is driven by a proper alignment of polymer and the SWCNTs energy levels, which enables charge transfer between them.[35] It is also known, that the CP backbone engages in $\pi - \pi$ interactions with SWCNT (wrapping), and its flexibility dictates diameter selectivity, *e.g.* more flexible structures are able to adjust their conformation to significant curvature of the surface of small-diameter nanotubes.[44,48,49] The CP side chains support isolation and dispersion of the wrapped nanotubes.[50] Their increase in length led to a higher concentration of extracted SWCNTs, but also compromised the polymer preference towards semiconducting nanotubes, presumably through generally stronger van der Waals interactions.[34] Too low molecular weight of the CP was found to lead to unstable dispersion, but on the other side, too high molecular weight coincided with the decrease in CP solubility and led to extraction of more than one SWCNT species.[47,51,52]

The organic solvent assures solubility of the polymer, its proper conformation and interactions with the SWCNTs. Its density should be lower than the density of the CNT bundles ($\sim$1.3 g/cm^3), to ensure their effective precipitation during centrifugation.[35] Usually, non-polar solvents such as toluene or xylene are used for extraction, because polar solvents fail to create a stable dispersion with polyfluorenes, and they were found to enhance the solubility of metallic SWCNTs. However, some polycarbazoles can extract s-SWCNTs in tetrahydrofuran (THF),[55] which shows that not all dependencies in the extraction systems are yet satisfactory explained. Additionally, please note that *e.g.* density or viscosity of the extraction mixture can be influenced by the solvent as well as molecular weight of the CP. This and similar dependencies hamper the possibility of understanding the exact role of polymer or solvent in the extraction system.

To evaluate and compare the results of extractions, two parameters are used, calculated based on the absorption spectra of the dispersions. First is chiral purity, also called selectivity, defined as the percentage of the desired chirality in the final dispersion. Second is yield, calculated as mass of extracted SWCNTs divided by the mass of the same SWCNTs in the source material. Both chiral purity and yield are affected by polymer/SWCNTs ratio,[40,50,53] sonication time and

temperature, centrifugation velocity etc. Proper selection of the process parameters leads to chiral purities of 80-90%,[39,40,46,56] but the extraction yield of chirally-selective extractions is still very low, oscillating around 1-3%. Fortunately, the SWCNT source material can be re-used for another cycles of extraction[39,57,58] which increases the yield. The recurrent CPE shows potential as a method of large-scale production of monochiral dispersions of SWCNTs, which was discussed in greater detail in the first publication presented in this thesis.

The last important aspect that needs to be brought to the reader's attention to ensure proper understanding of the described issues is the role of extracting polymer in the dispersion in context of the further processing of the SWCNTs. Precisely, should the excessive polymer be removed from the dispersion, or is it neutral or maybe positively influences further reactions or deposition on a substrate? Does the polymer influence the intensity of PL emission? In most papers, the CP removal is included in the methodology of preparation of monochiral SWCNT for chemical functionalization,[59–62] but the process is time- and resource-consuming. Additionally, significant part of the SWCNT material is usually wasted in this process. Some reports showed no significant differences between performance of SWCNT transistors printed with and without polymer excess.[63–65] Additionally, Mirka *et al.* suggested, that the excess of unbound polymer could help to reduce device-to-device uniformity.[65] Because of that, in this work, the polymer was not washed after extraction – meaning it was present in excess during functionalization. For comparison, several functionalization reactions were conducted using SWCNTs without the excessive polymer, but the PL emission intensity was lower and the SWCNTs were more prone to precipitation. The possible influence of the dispersant on further processes is still under investigation.

1.3. Careful defect implementation

As it was already mentioned, to obtain high-quality PL emission from the SWCNTs, their QY can be enhanced in chemical reaction of functionalization. This type of functionalization relies on covalent attachment of modifying groups on the surface of the SWCNTs, which introduces specific sp^3 defects, also called luminescent defects, quantum defects or organic color centers.[66] They lead to new electronic states in the structure of the SWCNTs, resulting with further red-shifted PL emission, with longer lifetimes and higher QY, assuming that the luminescent defect density is optimal (Figure 1.4a). The photophysics of these phenomena was studied lately and described thoroughly in the review articles on the topic.[17,67–70] Briefly, the confined 1D structure of the nanotube favors creation of excitons (bound electron-hole pairs), which are responsible for the major optical features. In pristine SWCNTs, the excitons are highly mobile and thus very likely to find quenching sites, such as the end of the nanotube or unintended defect in their structure. Quenched excitons do not contribute to PL emission, and abundance of quenching sites is the reason behind low QY of the SWCNTs. However, it was discovered, that

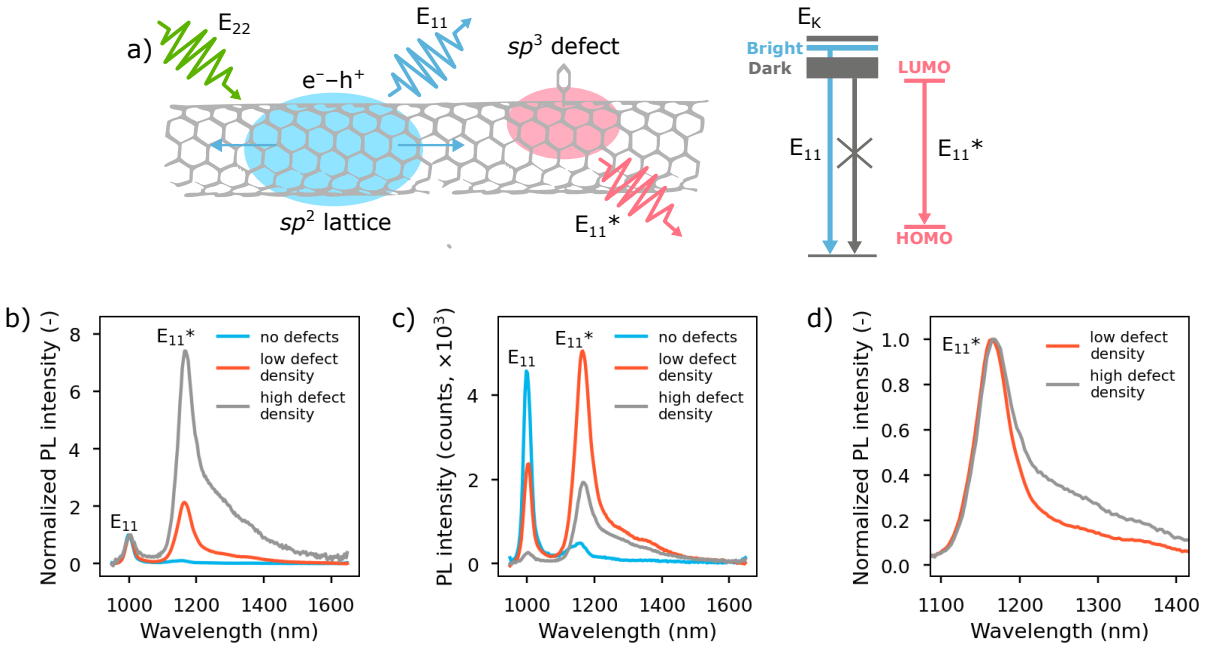

Figure 1.4. a) An illustration of the E_{11} emission originating from the excitons moving freely in the sp^2-hybridized lattice of carbon atoms in SWCNT and their energy levels; and E_{11}* emission of lower energy from the excitons trapped on the sp^3 defect. Both emissions are the effect of excitation at the E_{22} wavelength. The images were redrawn from reference.[71] b) PL spectra od the monochiral SWCNTs with different amount of luminescent defects, normalized to the maximum value of the E_{11} emission, for comparison of the defect densities. High defect density suppresses the overall intensity of PL emission (c) and compromises the PL emission homogenity (d).

the luminescent sp^3 defects can create new lower energy states, able to localize the excitons. The typical trap depth of 100–250 meV prevents escape to the quenching sites. The new states are optically active, giving rise to E_{11}* PL emission (red-shifted from the original E_{11} PL of the nanotube) and increasing the QY. In PL spectrum of a bulk sample, for pristine SWCNTs only E_{11} emission is observed, while modified SWCNTs show both E_{11} and E_{11}* emission features. E_{11}*/E_{11} area ratio increases with defect density, which was illustrated in Figure 1.4b, presenting PL emission spectra of pristine SWCNT (no defects), compared to SWCNTs with low and high defect densities.

Importantly, for optimal properties of modified nanotubes, the number of defect states must be limited. Excessive number of functional groups on the surface of the SWCNT decreases overall intensity of PL emission (Figure 1.4c), eventually leading to complete loss of the emissive properties. Several research groups estimated the defect density in the SWCNTs of maximum E_{11}* photoluminescence. Wang *et al.* found that there is approximately one defect per 20 nm length of (6,5) SWCNT.[71] Zaumseil *et al.* reported from 5 to 30 defects per μm of nanotube length,[69] however, for the highest degree of functionalization, an additional emission band, even further red-shifted than the E_{11}* was present. In general, high defect density promotes

the appearance of additional emission features on different wavelengths (Figure1.4d), which is undesirable for optical applications.

The wavelength of emission depends on the chemical composition of the attached functional group and its binding configuration. *E.g.* the (6,5) SWCNTs in water environment exhibited the E_{11}* PL emission at approximately 1120[72] or 1140 nm,[71] when its surface was modified with oxygen defects or aryl defects, respectively. Other quantum defect systems resulted with different emission wavelength.[73] Additionally, it was shown that the emission is further red-shifted if functionalizing groups have electron-withdrawing abilities, due to stronger perturbations in the π-electron network of the nanotube.[66,71,73–75] Strong red-shifts were obtained also upon divalent functionalization[75] (the groups were attached to two different carbon atoms in the SWCNT), which underscored the importance of bonding character. For the aryldiazonium functionalization, it was shown, that binding of the aryl group at one carbon site produces a reactive un-paired electron in 2- or 4- (*i.e. ortho* or *para*) configuration, which subsequently captures a proton, an OH group or another aryl group. Because of the geometry of chiral SWCNTs like (6,5), there are six possible chemically distinctive configurations of binding the additional group.[76] Each of them was assigned to different wavelength of PL emission in modified SWCNTs. To achieve this, experimental and theoretical approach (density functional theory, DFT) were simultaneously used to resolve the PL spectra[75,77] of SWCNTs with different functionalizing groups attached. Moreover, in specific conditions, next to exciton emission, the trion emission was also observed.[78] Because of the listed phenomena, the reactions of functionalization should be strictly controlled by selection of modifying groups, their concentration, temperature, time, type of solvent *etc.*, to ensure only one type of functionalizing groups, which guarantee a selective emission.

Several articles review luminescent functionalization methods,[79,80] in one of which Professor Janas proposed a distinction between chemical methods of introducing a photoluminescence defect into SWCNTs,[79] which was updated to include lately emerging methods of arylation and presented in Figure 1.5. The methods can be either inorganic or organic, regarding the type of functional group introduced. The inorganic approach is focused on oxidation, with the reactive species involving hydrogen peroxide,[81,82] ozone,[72,83,84] sodium hypochlorite,[85,86] unsatturated fatty acids[87,88] *etc*. Additionally, defect peaks can be introduced even in the absence of dedicated reactive species, upon high power sonication.[89] In this reaction H_2O_2 and hydroxyl radicals generated from water lead to decomposition of the surfactant molecules into reactive species, ready to attack the SWCNTs. This result underscores the importance of understanding the side reactions proceeding during functionalization, which will be further discussed in this work. The organic routes are even more diverse. Alkylation is possible through Billups-Birch reduction,[90] by using sodium naphtalenide,[91–94] or alkyllithium followed by alkylbromide,[95–98] *etc*. Further, arylation is possible through several different methods using haloanilines,[99]

phenylhydrazines,[100] sodium naphtalenide and iodobenzene[101] or azacrown-ethers[102] but the most explored path relies on introducing functional groups from diazonium salts.[61,71,76,103–108]

The investigations conducted using diazonium chemistry allowed to draw conclusions helpful in understanding the reactions of SWCNTs with other compounds as well. *E.g.* Piao *et al.* first showed a linear correlation between the optical trap depth and Hammett constant of a substituent to the aryl functional group,[71] which was consequently corroborated by other studies.[103,109] It allowed for very convenient manipulation of the defect emission wavelength and was also presented for functionalization with phenylhydrazines[100] or, in this work, with aryl peroxides. Further, it was demonstrated that the rotation of the functionalizing aryl group with respect to the nanotube has negligible effect on the optical spectrum.[76] Wang *et al.* developed methods of red-shifting the emission by controlling the steric sizes of the functional groups and postulated the co-existence of radical and carbocation mechanisms of reaction.[107] Saha *et al.* discovered, that using 'zig–zag' SWCNTs allows to narrow the emission bandwidth, because of geometrical restraints of these structures.[105] Moreover, estimation of luminescent defects density was conducted using diazonium-modified SWCNTs.[71,108,110] Despite this popularity, diazonium chemistry is most efficient in aqueous dispersions of surfactant-coated SWCNTs, which show lower chiral purities and worse film-formation properties than recently emerging polymer-wrapped SWCNTs in organic solvents. To utilize the potential of CPE, there arose a need for new methods of introducing the luminescent defects into SWCNT structure, which could be conducted in organic environment. First, Zaumseil *et al.* proposed a method of transferring diazonium salts into organic solvents. Using phase-transfer agent and a mixture of toluene and acetonitrile (4:1 vol.) they successfully introduced PL defects into (6,5) SWCNTs. This method is still used in their subsequent works.[106,110] Simpler protocols of functionalization, using compounds readily soluble in organic solvents were also presented,

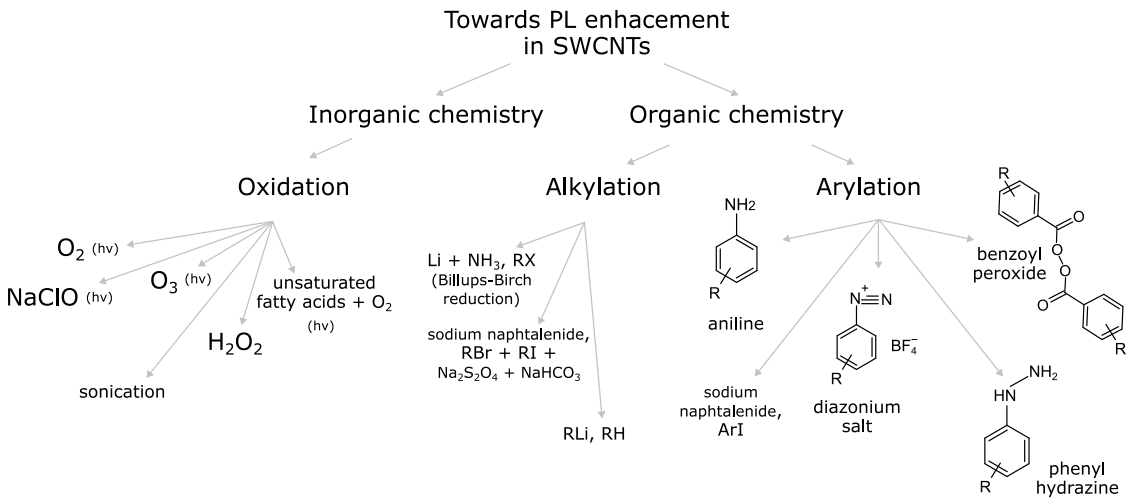

Figure 1.5. Schematic representation of different chemical routes to PL emission modification, redrawn from reference[79] with updated methods of arylation.

employing haloanilines,[99] phenylhydrazines[100] and aryl peroxides.[111] The latter was discovered by my team colleague and was also used in this work. In order to better understand the phenomena observed upon SWCNT modification with these compounds, an introduction to chemistry of the aryl peroxides, precisely benzoyl peroxide, was presented in the next section.

1.4. Chemistry of benzoyl peroxide (BPO)

Reactions with other radical species were already employed to photoluminescent functionalization of the SWCNTs,[85,89] proving that the radical chemistry can be harnessed to implement the sp^3 defects in controllable manner. On the other hand aryl peroxides are widely used chemical compounds. Among them, BPO is one of the most important in terms of applications, most often used as a polymerization initiator, curing agent or cross-linking agent. Importantly, BPO dissolves well in toluene and similar solvents (*e.g.* xylene, tetralin), which was convenient due to their effectiveness in the CPE process. The organic environment was not only compatible with the chiral extraction procedure, but also crucial to limit the influence of hydroxy radicals created from water molecules. Further control over the course of reaction was gained by optimization of the reaction conditions, *i.e.* radical initiator structure and concentration, temperature level, type of solvent and presence of oxygen and moisture. Understanding the chemistry of the BPO itself in these conditions was the first step towards gaining control over the formation of only one type of radicals (benzoyloxy radicals) and their incorporation into the structure of SWCNTs.

Aryl peroxides thermally decompose into radicals by homolytic cleavage of the O-O bond. Spontaneous thermal decomposition of BPO, most effective at high temperatures and low initiator concentrations, results in creation of two benzoyloxy radicals (Figure 1.6a, (1)). In 1946, Nozaki *et al.* demonstrated that, in different organic solvents, order of increasing rates of spontaneous BPO decomposition is as follows: highly halogenated solvents $<$ most aromatics $<$ most aliphatics $<$ ethers, alcohols, monohydric phenols $<$ amines.[112] For controllable reactions of functionalization, moderate rates of radical decay are preferred, so in this work, almost exclusively solvents from the first two groups were used. Further, the benzoyloxy radicals are prone to various further reactions, which can lead to the creation of other unreactive or reactive species. *E.g.* benzoyloxy radicals may lose carbon dioxide to give phenyl radicals (2),[113] which can attack the SWCNT, leading to additional bands in the PL emission spectra. Moreover, the benzoyloxy radical can induce the decomposition of the initial BPO molecule (3). In such reaction, called induced bimolecular decomposition, one benzoyloxy radical is formed, along with nonreactive residues ($e.g.$ CO_2, phenyl benzoate). Finally, free benzoyloxy radical can react with the solvent molecule by removal of an atom, leaving a new radical, *e.g.* the benzyl radical if toluene was used as a solvent (4). Other solvents were expected to produce different radicals, depending on their structure. In polymer chemistry, transferring a radical from an

initiator to a solvent molecule or other mediator (*e.g.* a chain transfer agent) is called chain transfer. Every solvent can be characterized by a chain transfer constant, which defines its susceptibility to forming secondary radicals. This process can be retarded by inhibitors, *e.g.* oxygen, although this inhibition effect is expected to be less significant in the solvents which already are slowing down the decomposition reaction rate.[112,114] The same as benzoyloxy radical, this solvent-originating radical can further induce bimolecular decomposition of the BPO molecule (5). For SWCNT functionalization, the formation of benzyl and phenyl radicals is undesirable, so the conditions favoring decarboxylation and chain transfer reactions should be avoided.

The control over the outcome of functionalization reaction can also be gained using the chemical modification of the radical initiator structure. Specifically, substituents attached to aromatic part of benzoyl peroxide structure alter its reactivity towards the SWCNTs and defect configuration.[71,98,109,115] In general, the substituents influence on the aromatic compound reactivity was quantified as Hammett σ constants. The more electron-attracting a substituent is, the more positive is its σ value (relative to H as 0.0). Conversely, the more electron-withdrawing substituent, the more negative is its σ value. The σ value depends not only on the substituent structure, but also its position in the ring (Figure 1.6b). This difference originates in the fact,

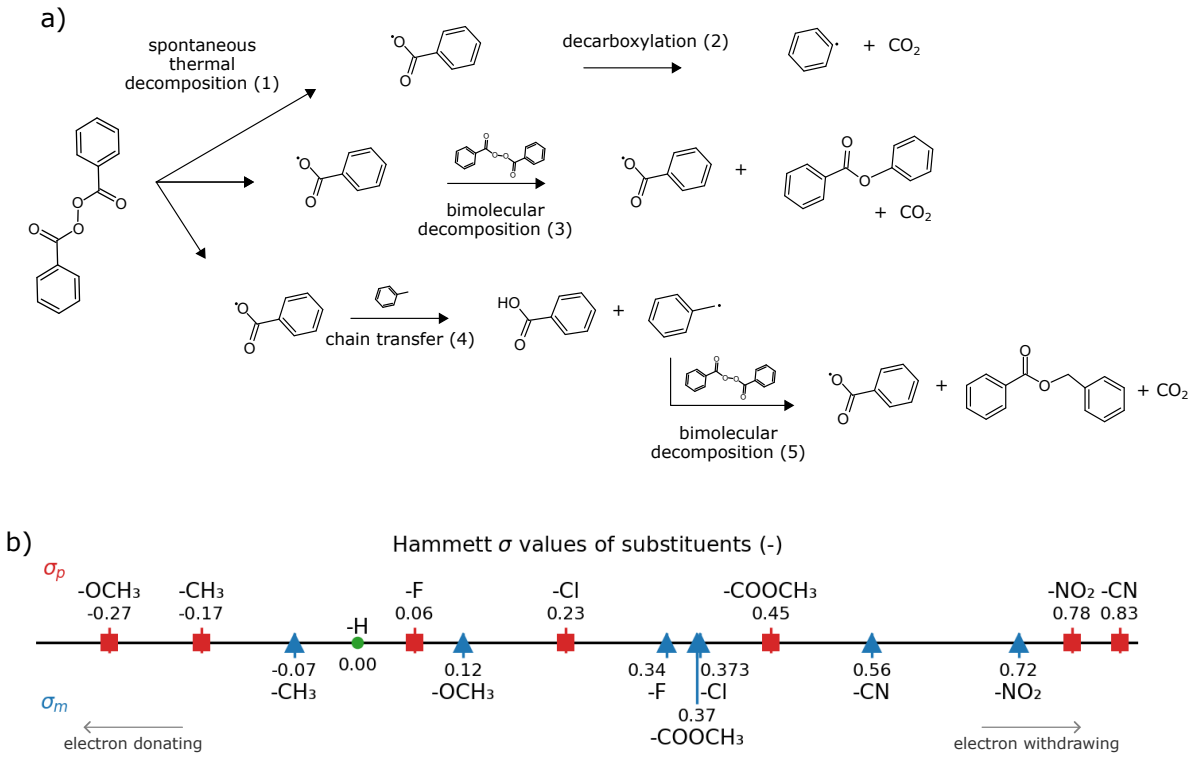

Figure 1.6. a) BPO decomposition pathways (full description in the text). Figure was copied form P2 and modified. b) Values of Hammett constant σ for selected substituents in *para*– (red squares) and *meta*– (blue triangles) configuration.

that for the substituents in *para* position (red), σ represents the net influence of both inductive ($-I$) and resonance ($-R$) effects, while for the *meta*$-$ substituents (blue), σ value corresponds to the inductive effect alone. The *ortho* substituents are not usually treated within the context of the Hammett equation because steric effects can interfere with the purely electronic effects, and these steric effects are highly variable from reaction to reaction. The derivatives of the BPO (with the substituents in 3- or 4- positions), showed a linear correlation between their Hammett constant σ and rate constant of spontaneous decomposition of the peroxide in dioxane.[116] Similar trend, only reversing for polar groups, was observed in acetophenone.[117] The authors explained these observations, by imagining the two benzoyloxy groups of the peroxide as dipoles, which can repel one another. The partial negative charges on the central oxygen atoms were increased with electron-rich substituents in the structure, characterized by lower σ values, leading to stronger repulsion and increasing the probability of decomposition. Analogically the charge was decreased upon using electron-poor groups (higher σ value), making the molecule more stable.[116]

These earlier findings were very helpful in the interpretation of the observed changes in PL emission spectra of the SWCNTs modified using BPO derivatives. Other than controlled decomposition of the substituted peroxide, another crucial aspect was the substituted benzoyloxy radical affinity towards the SWCNTs. Although some correlations of the aryl group structures and their reactivity towards the SWCNTs were already observed in case of diazonium salts,[61] this aspect was not discussed in details earlier.

2. Scope and Aim

Initially, the conjugated polyfluorenes PFO-BPy6,6' and PFO were used for the recurrent extraction of (6,5) and (7,5) SWCNTs, respectively, from commercially available chirally enriched SWCNT mixtures (**P1**). The polymers were synthesized in-house *via* Suzuki–Miyaura polycondensation. As the mechanism of these reactions is well documented in the literature and the syntheses were performed by colleagues of the authors, detailed descriptions of polymer synthesis are not included here. Instead, this work focuses on gaining deeper insight into the recurrent extraction process itself. In particular, the study addresses whether all polymer chains are effectively involved in SWCNT wrapping, whether polymer chains accumulate in the precipitate together with unsorted SWCNTs, whether the precipitated polymer can be recovered, how the extraction efficiency can be improved, and whether the quality of the extracted material changes over subsequent extraction cycles. This analysis enabled the identification of optimal parameters to enhance both the selectivity and efficiency of the extraction process, as well as to ensure the feasibility of recycling both the polymer and the sorted SWCNT material. The improved large-scale methods for producing near-monochiral (6,5) and (7,5) SWCNT dispersions are subject to patent protection in the Republic of Poland (**Pat1**). These methods were subsequently used to prepare hundreds of milliliters of a uniform starting material for SWCNT functionalization.

Thermal functionalization was performed using BPO in toluene (**P2**). A broad range of reaction conditions was systematically explored to optimize process parameters for the controlled introduction of sp^3 defects into the SWCNT structure. The reactions were carried out under varying levels of oxygen and moisture, as well as in different solvent environments, in order to evaluate their influence on the functionalization process. Based on literature reports, changes observed in the PL spectra of modified SWCNTs were correlated with the formation of distinct radical species arising from the activation of one or both BPO decomposition pathways. This approach provided deeper insight into the functionalization mechanism and enabled precise control over defect density, which is required to tailor the photonic properties of SWCNTs for specific applications.

The potential of BPO was further explored using a library of its in-house synthesized derivatives (the synthesis process will not be discussed here), with functional groups such as alkyl, alkoxyl, carbonyl, halide, nitrile, or nitro, in 3- or 4- position on the benzyl ring. This alteration significantly influenced the reactivity of the peroxide towards the SWCNTs as well as spectral shape of PL emission. The effects related to resonance stabilization were observed

for derivatives with functional group in 4- position. Importantly, an insight was gained into why the electron-withdrawing reactants are optimal for SWCNTs functionalization for optical applications (**P3**).

This work further elucidate the reaction mechanism of s-SWCNT and the causes of their affinity towards certain functional groups. Secondly, it presents a new scalable method of tuning the PL spectra, which is compatible with polymer-extracted chirally selective SWCNTs. The obtained results significantly contributed to the development of the chemical sciences and expanded our understanding of the selective isolation and covalent functionalization of (6,5) and (7,5) SWCNTs.

3. Experimental

3.1. Materials

CNTs. This study was carried out using (6,5)-enriched CoMoCAT SG65i SWCNTs (Sigma-Aldrich, product number: 773735).

Solvents: toluene (Alfa Aesar, cat. number: 19376.K2, CAS: 108-88-3, spectrophotometric grade, purity: >99.7%), *p*-cymene (Alfa Aesar, cat. number: A19226.AP, CAS: 99-87-6, purity: >97%), hexane (Alfa Aesar, cat. number: L09938.AK, CAS: 110-54-3, purity: 99%), cyclohexane (Alfa Aesar, cat. number: A16070.0J, CAS: 110-82-7, purity: 99%), decahydronaphthalene (decalin, Alfa Aesar, cat. number: A13883.AP, CAS: 91-17-8, purity: 98%, cis + trans), tetrahydronaphthalene (tetralin, Fisher Chemical, cat. number: T/0850/08, CAS: 119-642, purity: >97%), tetrahydrofuran (THF, Alfa Aesar, cat. number: L13304.AP, CAS: 109-99-9, purity: 99%), acetonitrile (Alfa Aesar, cat. number: A19862.AP, CAS: 75-05-8, purity: >99%), diphenyl ether (Alfa Aesar, cat. number: A15791.36, CAS: 101-84-8, purity: 99%), *o*-xylene (Alfa Aesar, cat. number: A11358.AP, CAS: 95-476, purity: 99%), benzene (Chempur, cat. number: 111625000, CAS: 71-43-2) and *o*-dichlorobenzene (DCB, Fisher Chemical, cat. number: D/1600/15, CAS: 95-50-1, extra pure), were used as supplied, without additional purification or drying, unless stated otherwise.

Reagents: BPO (VWR Chemicals, cat. number: L13174.30, CAS: 94-360, purity: 97% (dry weight), moistened with 25% water), tetramethylammonium hydroxide (TMAH, Thermo Scientific, cat. number: 11327368, CAS: 75-59-2, electronic grade, purity: >99.9%) were also used as supplied, without additional purification or drying, unless stated otherwise.

Extracting polymers: PFO (poly((9,9-dioctylfluorene)) and PFO-BPy6,6' (poly(9,9-dioctylfluorene-alt-6,6'-bipyridine)) – structures in Figure 1.3 – were prepared using the Suzuki coupling method, their structure was confirmed by ^{1}H NMR spectroscopy and the macromolecular parameters were examined by SEC. As mentioned earlier, the details of synthesis are not included here, the curious reader can found them, along with the results of SEC and NMR analysis in the paper **P1**.

Aryl peroxides Other than the commercial BPO, in-house synthesized BPO was prepared, along with 14 of its derivatives (structure is presented in Figure 1.5, benzoyl peroxide). The derivatives were symmetrically mono-substituted with groups: OCH_3-, CH_3-, $COOCH_3$-, F-, Cl-, CN- and NO_2-, in 3- and 4- positions in the benzene ring. The structure was confirmed by

Table 3.1. Comparison of materials and parameters used in CPE process conducted in small (research) and big (production) scale.

Scale	SWCNTs	PFO-BPy6,6' / PFO	Toluene	Bath Sonication	Tip Sonication	Centrifugation
Small	1.5 mg	6 / 9 mg	5 mL	5 min	30 W, 8 min	10,000 rpm, 3 min
Big	6.0 mg	24 / 36 mg	20 mL	10 min	50 W, 16 min	10,000 rpm, 5 min

^{1}H NMR spectroscopy. The details of synthesis and characterization are also not included here, the curious reader can refer the paper **P3**.

3.2. Methods

Preparation of (6,5) and (7,5) SWCNTs. The near-monochiral (6,5) and (7,5) SWCNT were collected by recurrent CPE. In a typical suspension process, 6 mg of PFO-BPy6,6' or 9 mg of PFO were dissolved in 5 mL of toluene. The solution was then transferred to a glass vial with 1.5 mg of pre-weighted SWCNTs. The mixture was homogenized in an ice-cooled bath sonicator (POLSONIC, SONIC-2, 250 W) for 5 minutes, until the solution was black and thick. Then, tip sonication (Hielscher UP200 St ultrasonic generator) was conducted at a power of 30 W for 8 min, while the mixture was cooled in an ice bath to keep temperature of approximately 5 °C. This enabled polymer-wrapping of selected SWCNTs. After sonication, the thick suspension was transferred to a conical tube and centrifuged (Eppendorf 5804 R) for 3 min with 10,000 rpm (15,314 $\times$ g) to remove the bundled SWCNTs and polymer aggregates. Then, 90% of the supernatant (containing the close-to monochiral SWCNTs wrapped in polymer) was collected and characterized by optical spectroscopy. On the other hand, 5 mL of toluene was added to the SWCNT soot remaining in the conical tube, mixed and transferred to a vial for the next extraction cycle. Polymer was added when needed, based on the absorption spectra.

Then, this basic method was up-scaled, by increasing the amount of SWCNT source material, CP and solvent 4 times, and increasing sonication time and power (Table 3.1). Based on literature, further up-scaling is possible.[39]

Verification of chiral purity. Absorption spectra of the extracted SWCNTs were usually recorded in wavelength range from 280 to 1100 nm, due to device availability (Hitachi U-210 spectrometer). However, the E_{11} emission of *e.g.* (7,6) or (10,2) SWCNTs are further red-shifted, so upon each modification of the extraction strategy, wider spectra in wavelength range up to 1250 nm were collected (Perkin Elmer Lambda 1050 spectrophotometer), covering all E_{11} and E_{22} bands of all the SWCNT species present in the starting material. Measurements were made with pure toluene as a reference. For the SWCNT content analysis, the absorption spectra were baseline-corrected and deconvoluted using PTF Fit software.[118] SWCNT concentrations (c) were calculated therein using Lambert-Beer's law and

Table 3.2. Parameters of the SWCNTs present in CoMoCAT SG65i material, used for deconvolution of the absorption spectra: diameter d, chiral angle θ, wavelengths λ_{11} and λ_{22} of the E_{11} and E_{22} optical transitions, as well as molar and weight-to-volume absorptivity constants ϵ_{11}.[119]

(n,m)	d (nm)	θ (°)	λ_{11} (nm)	λ_{22} (nm)	ϵ_{11} (M^{-1} cm^{-1})	ϵ_{11} ($(\mu g/mL)^{-1}$ cm^{-1})
(5,4)	0.620	26.3	855	503	5200*	0.43*
(6,4)	0.692	23.4	893	598	5200	0.43
(6,5)	0.757	27.0	996	586	6700	0.55
(7,3)	0.706	17.0	1012	525	6600	0.55
(7,5)	0.829	24.5	1044	665	4500	0.39
(7,6)	0.895	27.5	1140	668	5500	0.47
(8,1)	0.678	5.8	1061	491	5200*	0.43*
(8,3)	0.782	15.3	972	685	4900	0.43
(8,6)	0.966	25.3	1193	738	3300	0.27
(9,1)	0.757	5.2	932	711	7700	0.64
(10,2)	0.884	9.0	1073	757	3400	0.29

* Due to no parameters available in literature, values for the closest-diameter (6,4) SWCNT were used here. These chiral species were very rare, so this simplification did not influence the calculations in significant way.

chiral-specific absorptivity values (ϵ), determined by Weisman *et al.*[119] The exact values used in this study are presented in Table 3.2. Figure 3.1 shows exemplary fitted spectra of the un-sorted SWCNTs, as well as selectively isolated (6,5) and (7,5) species.

Normalization by dividing by the maximum intensity of the E_{11} transition, allowed for convenient comparison of chirality distribution in different dispersions. Chiral purity (p) was expressed as the concentration of a particular compound (n,m) divided by the sum of concentrations of all SWCNTs extracted in a specific cycle. Mass of the SWCNTs extracted in a particular cycle was calculated by multiplying concentration by volume of the supernatant after centrifugation. This volume was usually about 0.7-0.8 of the initial solvent volume due to the binding of a portion of the solvent by the SWCNTs sludge. The extraction yield (y) was calculated as a mass of extracted SWCNTs divided by its initial mass in the starting material (*e.g.*, the starting 1.5 mg of raw SWCNTs used for purification contain approx. 0.52 mg of (6,5) SWCNTs).

Thermal functionalization of the SWCNTs. Initially (**P2**), 0.5 mL of (6,5) SWCNTs derived from standard extraction with PFO-BPy6,6' in toluene were diluted to 0.3 cm^{-1} (E_{11} (6,5) absorbance peak maximum). Commercially available BPO was dissolved in an identical volume of toluene (0.5 mL) to achieve the necessary concentration. The indicated components were then combined in a glass vial and immersed in a hot bath kept at 40, 70, 85 or 100 °C. After an hour, the samples were removed, cooled down to room temperature, and characterized. For the lowest temperature level, the reaction time was elongated to 24 hours after initial experiments, due to very low reaction rate. To establish the role of oxygen in the reaction, the substrates and subsequently the mixture were flushed with argon prior to reaction and kept sealed till the

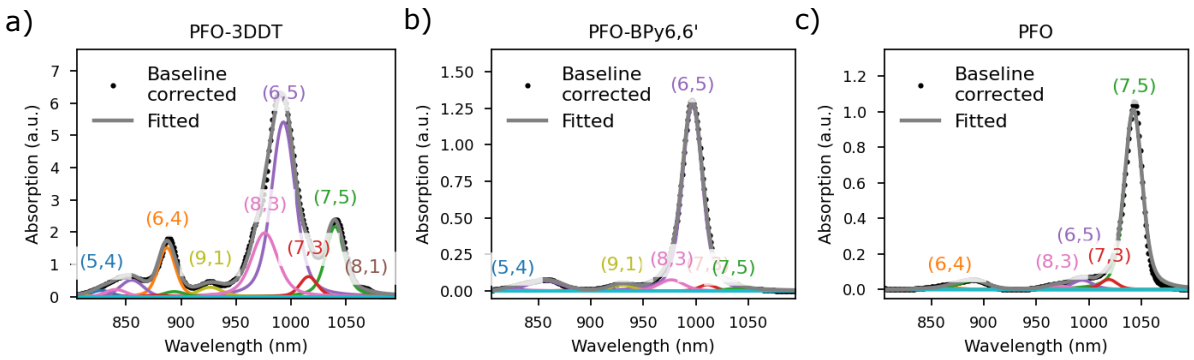

Figure 3.1. UV-Vis spectra fitted with the Voigt peaks for identification and amount calculation of each chirality. a) Un-sorted SWCNT mixed material, extracted using non-selective polyfluorene PFO-3DDT. Extraction using selective polymers b) PFO-BPy6,6' and c) PFO resulted in close-to-monochiral dispersion containing mostly the (6,5) or (7,5) species, respectively. Figure was copied from reference P1.

measurements. The influence of moisture was examined by i) drying the components (SWCNT dispersion in toluene and BPO dissolved in toluene or other organic solvent) with molecular sieves (4 Å) prior to the reaction or ii) addition of water to the mixture. The amount of water in the samples was determined using Karl Fischer titration, but these experiments and analysis are not described here. Different organic solvents were used instead of toluene to dissolve BPO, which allowed to observe functionalization in mixed-solvent environment (toluene from dispersion 1:1 vol. with co-solvent used for the BPO).

To compare the affinity of the in-house synthesized BPO derivatives towards the SWCNTs (**P3**), initial SWCNT concentration was increased to 0.8 cm^{-1} for the (6,5) chirality. This was necessary to observe the PL emission when modification was conducted using very reactive compounds (*e.g.* 4-$COOCH_3$-BPO, 3-CN-BPO) and also improved the functionalization repeatability. Reaction time was increased to 3 hours in case of (6,5) SWCNTs, because in some cases it allowed to obtain selective PL spectra using lower concentration of the radical initiator, which was desirable. For the less reactive (7,5) SWCNTs, up to 6 hour-long reactions were conducted. Reaction volume was increased from 1 to 2 mL to produce more functionalized SWCNTs and enable additional characterization; several reactions were conducted in both volumes for comparison and no significant differences in the reaction progress were observed.

To enable comparison between different BPO derivatives influence on different SWCNT chiralities, molar concentration of the (6,5) SWCNT was calculated as the maximum absorption divided by molar absorptivity value ϵ_{11} (Table 3.2). Molar concentration of the SWCNTs was kept constant in all reactions. The radical initiators were used in several constant molar concentrations (0.16, 0.32, 0.63, 1.25, 2.5 mM *etc.*). This way, it was possible to calculate the molar ratio of the BPO derivative towards the SWCNTs, represented as [R-BPO]/[CNT] (3:1, 5:1, 11:1, 21:1, 42:1 *etc.*).

Verification of the functionalization degree. First and most important characterization method were PL excitation–emission maps. They were collected with a ClaIR plate reader (Photonetc. Inc.) equipped with supercontinuum laser EVO HP EU-4 (NKT Photonics) and bandpass filter LLTF Contrast (NKT Photonics). The following settings were used for analysis: exposure time 100 ms, excitation range 460–900 nm, emission range 950–1650 nm. For PL measurements, SWCNTs were diluted so that their concentration in the measured samples was low, *i.e.*, 0.27 mg mL^{-1} (optical density of 0.2 cm^{-1} in E_{11} absorbance peak maximum in case of non-functionalized (6,5) SWCNTs) to avoid the inner-filter effect.[120] The PL spectra were extracted from the PL excitation–emission maps for the 574 nm excitation wavelength in case of (6,5) SWCNTs and 653 nm in case of (7,5) SWCNTs; normalized to the E_{11} or E_{11}* intensity for spectral shape comparison and fitted with a set of Voigt functions using self-developed Python scripts (Figure 3.2). The area ratio of all defect-induced peaks to the E_{11} peak was used for the estimation of the relative defect density implanted in the SWCNTs.

For comparison, the intensity ratio of defect induced D peak to G peak in Raman spectra was also used to measure the defect density in the SWCNTs. To obtain Raman spectra of the modified SWCNTs, it was necessary to prepare highly concentrated dispersions for drop-casting. The solvent excess was removed by centrifugation as follows. At least 1 mL of a sample containing the SWCNT suspension (with E_{11} absorption in the range of 0.3–0.4 cm^{-1} for pure SWCNTs) was mixed with 0.2 mL methanol (to promote precipitation of the SWCNTs) in a 2 mL conical tube and centrifuged. The supernatant generated from each sample was discarded after it was confirmed using PL excitation emission mapping that it did not contain SWCNTs. The SWCNT material deposited in the conical tube was redispersed in 0.2 mL toluene by a bath sonication (3 min) and subsequently drop-casted on a glass substrate for characterization. The samples were characterized using a Renishaw inVia Raman microscope

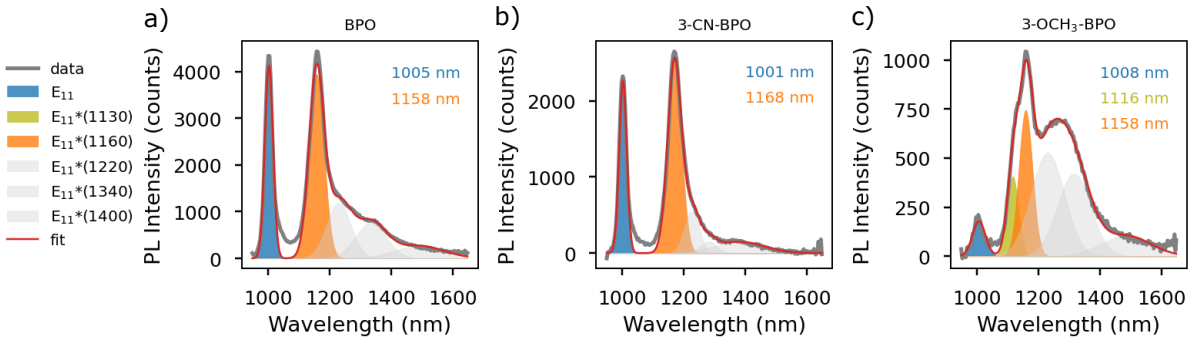

Figure 3.2. Exemplary PL spectra of functionalized SWCNTs with visualization of the set of model Voigt peaks used in this work. Initial spectral positions of the defect peaks are shown in the legend, and the positions of fitted peaks are shown in plots as examples. The results obtained with this approach were used to calculate E_{11} and E_{11}* at ~1130 and ~1160 nm peaks' positions and FWHM values. As a result, it was possible to track the occurrence of the indicated peaks. The structure and positions of further peaks are not elucidated yet. Figure was copied from reference P3.

equipped with a 50 objective (Leica). The spectra were baseline-corrected before calculating the I_D/I_G intensity ratios.

To provide a semi-quantitative assessment of the brightening effect upon functionalization, relative PLQY measurements were performed using IR-1061 infrared dye as a reference. This approach enabled a reliable comparison of emission efficiencies between pristine and functionalized SWCNTs under identical conditions. The detailed methodology and complete datasets are reported in **P3,** SI.

In addition, Fourier-transform infrared (FTIR) spectroscopy was employed to confirm the presence of newly introduced functional groups into SWCNTs (detailed methodology and complete datasets are reported in **P3,** SI). It should be mentioned however, that FTIR spectroscopy was also conducted by other authors of the publication.

4. Results and discussion

4.1. Improved method of chiral sorting of SWCNTs using recurrent conjugated polymer extraction (CPE)

The system of recurrent CPE was developed by other researchers and effectively used for selective extraction of the s-SWCNTs[36,43,56,57,121] as well as close-to monochiral SWCNTs,[39,52,53] however in the latter case, the polymer affinity to certain SWCNT species was compromised during the study. When single extraction is conducted, using enriched SWCNTs (such as CoMoCAT SG65i) and polyfluorenes in organic solvents, commonly chiral purities of 80–90% are obtained, which is comparable to much more expensive and complicated chromatographic methods. On the other side, the reported yields of single extraction of the (n, m) SWCNT did not exceeded 2-3%, leaving an abundance of the targeted species in the starting material. The recurrent CPE was developed as a method of improving isolation yield. The idea is, after finished isolation cycle (sonication and centrifugation) the supernatant containing monochiral SWCNTs was set aside and the remaining SWCNT sludge was poured with fresh portion of solvent (with the selective polymer if necessary) and again sonicated and centrifuged to isolate subsequent portion of the chirally selected SWCNTs, thus increasing the effectiveness of the process. Before the research carried out by me, up to 4 cycles of this process were reportedly conducted to isolate the (6,5) SWCNT, reaching 10% extraction yield.[39]

In this work, the (6,5) and (7,5) were both recurrently extracted using PFO-BPy6,6' and PFO, respectively. I conducted a series of experiments along with calculations, based on fitting the absorption spectra of the SWCNTs' dispersions with series of Voigt functions. Analysis of the obtained results allowed for selection of the process parameters with the biggest influence on chiral purity and yield of extraction. Complete extraction system was illustrated in Figure 4.1. It included partial re-cycling of the polymer and solvent after each cycle, by vacuum filtration of the close-to-monochiral dispersion through PTFE membrane. In this process, the polymer-wrapped SWCNTs are stopped by the filter and can be redispersed in a fresh portion of toluene, while the filtrate contains the CP dissolved in toluene, which can be used effectively for further extraction cycles. Each route of the system was practically implemented during this study.

New extraction strategy relied on deliberate addition of large excess of the CP. Usually, the CPE was conducted using between 0.5:1 to 1.5:1 weight ratio to the SWCNTs,[39,53] but here it was increased to 4:1 and 6:1 for PFO-BPy6,6' and PFO, respectively. The large excess of polymer

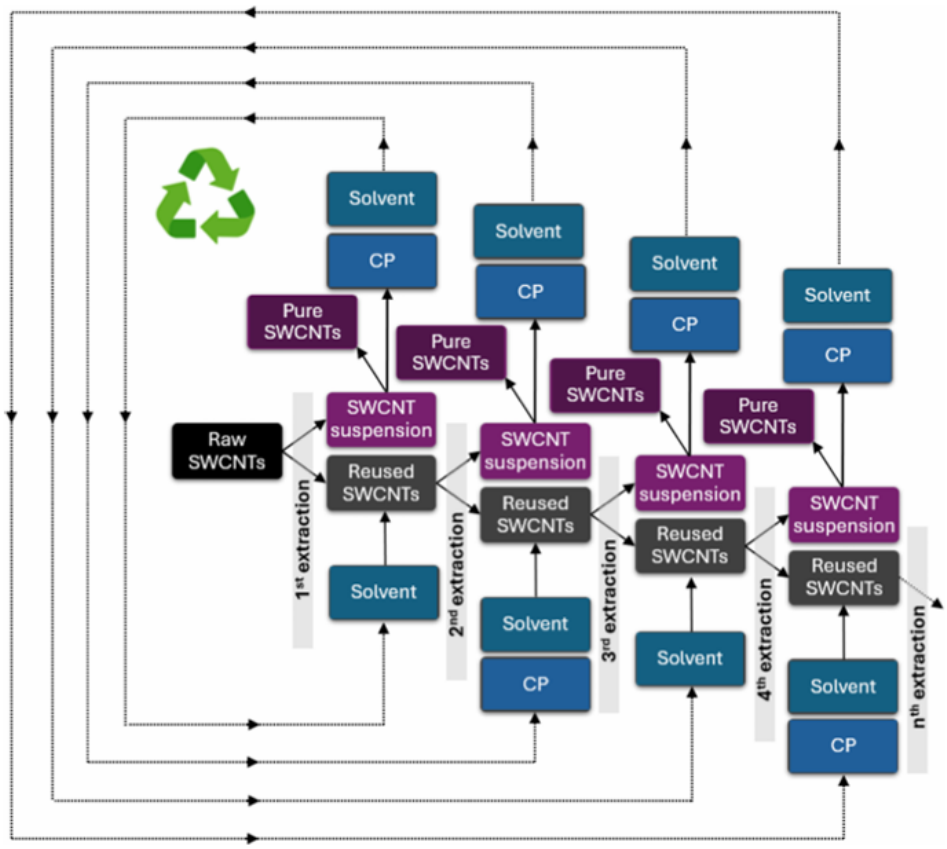

Figure 4.1. Process of multistep CPE. The initial process of extraction consumed raw SWCNTs and fresh CP solution. It resulted in a close-to monochiral SWCNT dispersion. Since in each cycle a large portion of the valuable material is precipitated in the postprocess sludge due to centrifugation, subsequent extraction cycle is required. Either pure solvent or a CP solution of lower concentration is added to extract the next portion of close-to monochiral SWCNTs from such solid residue. When indicated, the selectively extracted SWCNT fractions were cleaned by membrane filtration to remove excess polymer. The recovered CP was then collected and recirculated for use as a dispersant in subsequent SWCNT extraction cycles whenever specified. Figure was copied from reference P1.

allowed to obtain high chiral purity (p) of the nanotube dispersions (in the initial cycle, p was 85 and 91% for the (6,5) and (7,5) respectively). Precipitated after centrifugation, the polymer was successfully released into toluene during the next extraction stages, effectively wrapping selected SWCNTs. Because of that, only small additions of the CP in the subsequent stages were sufficient to continue the extraction with a satisfactory yield (y), so after multiple cycles, overall polymer usage was comparable to other strategies. Another advantage of using high initial CP/SWCNT weight ratios was significantly shorter sonication and by that, lower energy consumption comparing to other methods.

Although y was increasing with each cycle simply due to isolation of the additional portion of the (n, m) SWCNTs, after 13 cycles p deteriorated in both PFO-BPy/(6,5) and PFO/(7,5) systems down to 49 and 23%, respectively. Significantly, at that moment the chirality distribution was very similar to the initial CoMoCAT material, meaning both PFO-BPy6,6'

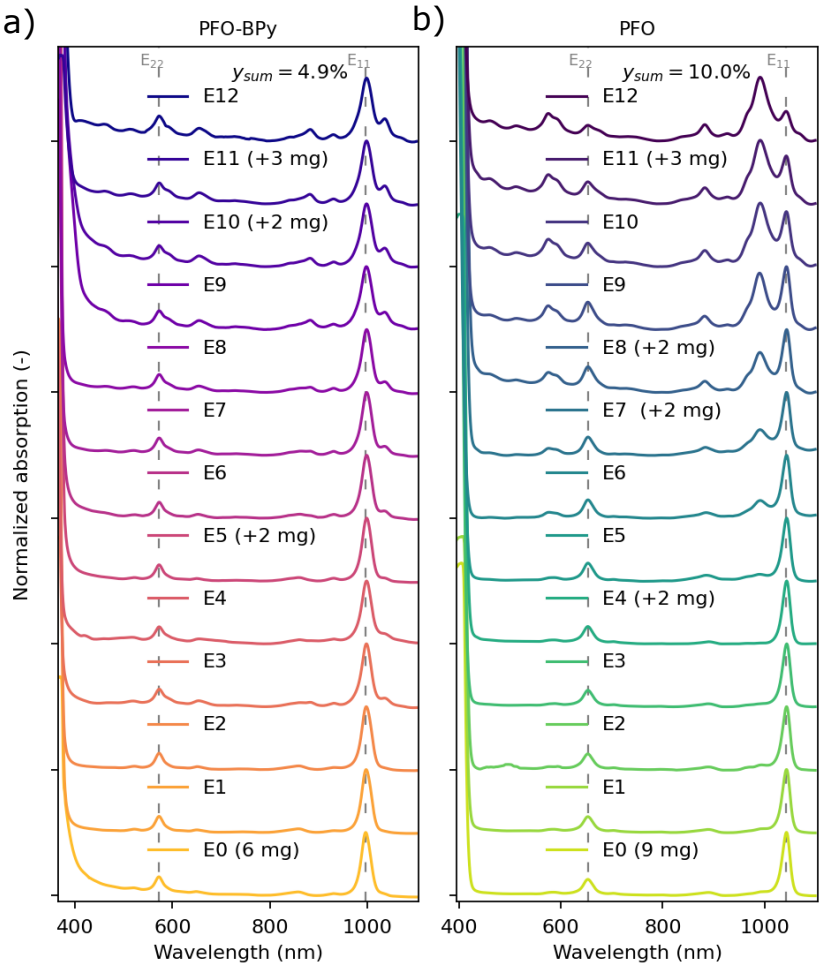

Figure 4.2. Normalized absorption spectra of 13 subsequent cycles of extractions from (a) PFO-BPy6,6' and (b) PFO in toluene, starting from initial extraction E_0. Dashed lines mark E_{11} and E_{22} optical transitions of $(6,5)$ and $(7,5)$ SWCNTs, respectively. Additional CP portions added to the subsequent cycles of extractions are marked with (+X mg). Cumulative yield y_{sum} shows the percentage of SWCNTs extracted from all extraction cycles. The spectra were offset to facilitate a comparison of chiral distribution. Figure was copied from reference P1.

and PFO lost their ability to discriminate by chiralities. The absorption spectra, normalized to clearly show chirality distribution were presented in Figure 4.2. Probable reasons to the observed gradual chirality loss include not-optimal macromolecular parameters of the CPs. Due to scarce control over their synthesis, they exhibit high dispersity Đ, meaning large spread between the weight- and number- average molecular weights (M_w and M_n, respectively). This means, such materials contain significant amounts of polymer chains, which are either too short or too long to effectively wrap the SWCNTs. Specifically, too long fractions tend to accumulate in the re-cycled sediment with the SWCNTs, leading to deterioration of the source material, explaining the observed selectivity loss. This finding underscores the need for better understanding of the CP synthesis. The above described observations allowed to further improve the yield (from 5% to 25%) and chiral purity. To consume the polymer more

efficiently, the sonication temperature was increased from 5 to 35 °C and sonication time was elongated from 8 to 16 minutes. Then the repeatability and scalability of the process was proven by differing the amount of the source material (CP/SWCNT weight ratio was kept constant) and solvent, as well as polymer molecular weight. High (M_n = 50.4 kg mol^{-1}, Đ = 2.3) and medium (M_n = 35 kg mol^{-1}, Đ = 2.8) molecular weight polymers were effectively used in toluene, upon proper selection of the sonication and centrifugation parameters.

Moreover, due to environmental considerations, toluene was replaced with more sustainable, but structurally similar *p*-cymene.[122] Successful recurrent isolation of the high-purity (6,5) SWCNTs in this solvent was conducted using PFO-BPy6,6' of low molecular weight (M_n = 6.3 kg mol^{-1}, Đ = 1.6) while for medium molecular weight polymer both *p* and *y* were low, due to worse solubility of the polymer in this solvent. This showed, that the recurrent CPE method can be adapted to the requirements of 'green' chemistry.

Washing off the polymer, as mentioned in the introduction, is not certainly necessary, but in large-scale production, it could anyway be useful to be able to re-use the free polymer chains present in the dispersion. This work shows such re-cycling is possible in case of PFO-BPy6,6' and PFO, as it was earlier proved for imine-based polyfluorene[123] and polycarbazole.[57,124] By simple filtration, polymer-wrapped SWCNTs were separated from the free polymer chains, and the latter were re-used in one of the further extraction cycles. It appeared, that the re-cycled CPs are in general of lower molecular weight than their as-synthesized counterpart, probably due to the consumption of the optimal-length chains by the SWCNTs and sedimentation of the long chains. When too short CP was used (PFO-BPy6,6', M_n = 1.55 kg mol^{-1}, Đ = 4.2), the extraction was unsuccessful, which again suggest the necessity for improved methods of the CP synthesis, allowing to better control their molecular weight.

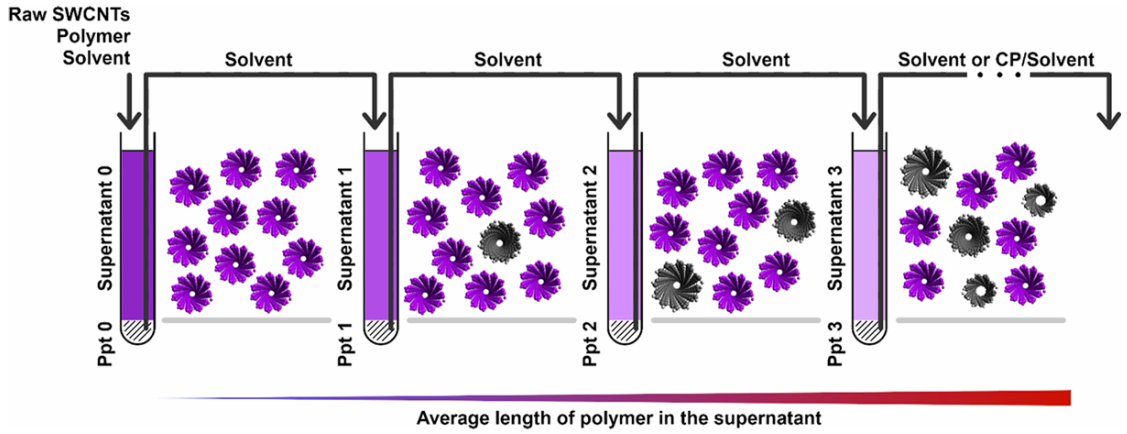

Figure 4.3. Proposed mechanism of reuse of the SWCNTs slurry leading to prolonged extraction of the (6,5) SWCNTs (marked in violet) from other chiralities (gray). Simultaneously, large molecular weight fractions of the CP are gradually deposited in the supernatant. Ppt – precipitate. Figure was copied from reference P1.

The proposed mechanism that accounts for the observed behavior is illustrated in Figure 4.3. During the sonication–centrifugation process, along with the wrapped SWCNTs, the polymer chains in either unbound form or aggregated as β-phase[125] were driven into the sediment. When this residue was reused, the accumulated polymer material could be reactivated and participate again in wrapping the SWCNTs during subsequent sonication steps. Because the low–molecular-weight fractions dissolved most readily, they were predominantly present in the supernatant during the initial extraction cycles. With each successive extraction, however, the proportion of long, nonselective polymer chains increased in both the sediment and the supernatant. As a result, at later extraction stages, the overall chiral selectivity was diminished.

The presented approach, capable of reclaiming all three components of the extraction system, *i.e.* SWCNT, CP and solvent, is a considerable step towards the sustainable and large-scale methods of chiral sorting of SWCNTs.

4.2. Modification of photoluminescent (PL) emission of the SWCNTs using BPO

The close-to monochiral s-SWCNTs are promising for photonics due to their selective NIR emission spectra. Their intrinsically low PLQY can be enhanced by functionalization, specifically the creation of luminescent sp^3 defects. Here, it was obtained by the covalent bonding of radicals, originating from thermally decomposed BPO, to the (6,5) SWCNT. This method was first proposed by the authors colleagues[111] and further developed in this study.

First, PFO-BPy-wrapped (6,5) SWCNT was reacted with BPO in toluene, in broad range of temperatures (from 40 to 100 °C) and radical initiator concentrations (from 0.5 to 15 mM). After the reaction, PL spectra of the SWCNTs contained, next to the original E_{11} emission (∼1000 nm wavelength), also defect-induced E_{11}* peaks (Figure 4.4). Most common defect resulted with E_{11}* peak at ∼1158 nm wavelength and was therefore assigned to the attachment of benzoyloxy radicals, which can be described as a SWCNT–O–C(=O)–R. Increase in the E_{11}*/E_{11} peak area ratio corresponded to increasing density of defects on the SWCNTs' surfaces. For a given temperature, defect density increased linearly with BPO concentration (Figure 4.5a), which enables good control over the reaction progress. In the same time, for a given concentration, the increase with temperature was fitted with exponential curve (Figure 4.5b). This was explained by the fact, that upon temperature increase, the defect formation accelerated when both decomposition pathways (uni- and bimolecular) occurred. When high temperature (100°C) was combined with significant concentration of the radical initiator (>3.8 mM), additional emission features were observed (Figure 4.4c), which was associated with the attachment of different functional groups, originating from radical recombination or radical transfer. In general, good control over the defect density was obtained upon using elevated temperature

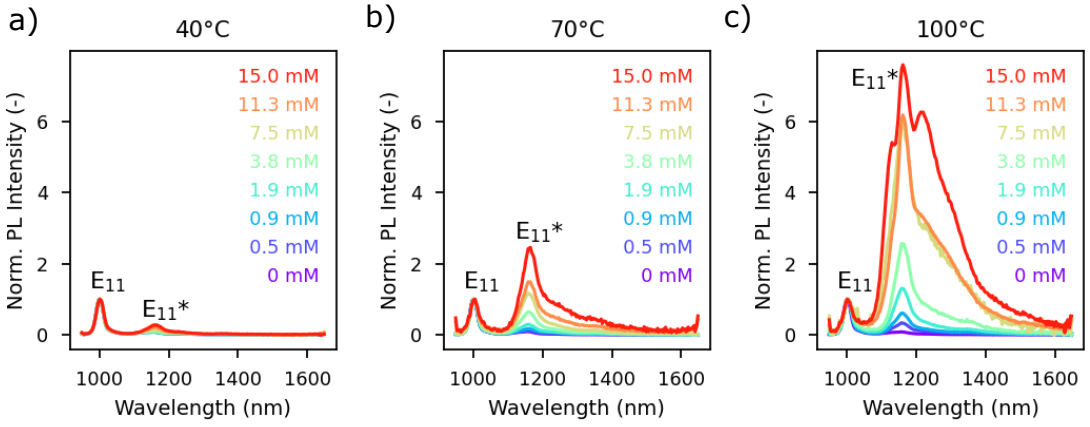

Figure 4.4. Normalized PL spectra of (6,5) SWCNTs functionalized using various concentrations of BPO from 0.5 to 15.0 mM. The spectra were registered after the reaction conducted at a) 40, b) 70, c) 85 and d) 100 °C for 1 hour. Excitation wavelength was 574 nm. Figure was copied from reference P2 and modified.

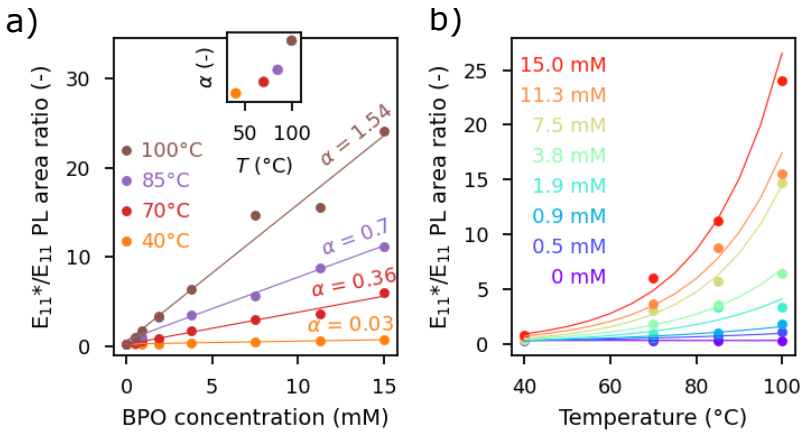

Figure 4.5. The ratio of E_{11}*/E_{11} integrated intensities of light emission as a function of: a) employed BPO concentrations for various temperature levels with linear fits (the inset illustrates the change in the slope a of the linear fit function as a function of temperature); b) temperature for different BPO concentrations with exponential fits. Figure was copied from reference P2.

(70-100 °C) and limited initiator concentration (<3.8 mM). This showed that considerate choice of the conditions, especially limited of the BPO concentration, allows for controlled modification of the PL spectra.

The radical formation mechanism is prone to environmental factors such as presence of oxygen and moisture. Although functionalization in organic solvents is considered free from the water-originating aggressive hydroxyl radicals (·OH), the moisture can be absorbed during storage or preparation, or present in the commercially available BPO as a stabilizer. Importantly, solubility of water in toluene increases with temperature,[126] which increases the probability of implementing various defects into the SWCNT structure in harsh reaction conditions. The ·OH radicals can attack the SWCNTs or BPO or its by-products, leading to formation of secondary radicals and as a consequence additional PL emission features. Oxygen, on the other hand, can retard the BPO decomposition and in most cases it inhibits the radical pathways.[127,128] To establish the effect of these environmental factors on the functionalization reaction course, SWCNT grafting was carried out: in the absence of oxygen, meaning that samples were flushed with argon ('–O_2'), in the absence of water, *i.e.* dried with molecular sieves ('–H_2O') or with the intentional addition of water ('+H_2O') (details in Experimental Section). The reaction outcome was different for each version of the procedure, especially large differences were observed when it was conducted at high temperature of 100 °C (Figure 4.6a). Spectrum of the SWCNTs prepared 'in air', meaning in standard conditions, without flushing with argon nor drying, consisted of several different features: E_{11} at 1005 nm, E_{11}* with two peaks at 1130 and 1160 nm, respectively, and lower intensity emission peaks (supposedly 3 different) in 1200–1450 nm range. Removing the oxygen from the reaction ('–O_2') was proven to have a very subtle impact on the reaction course in the organic environment. Creation of the main defect peak (1160 nm) was practically insensitive towards the oxygen content, however, the

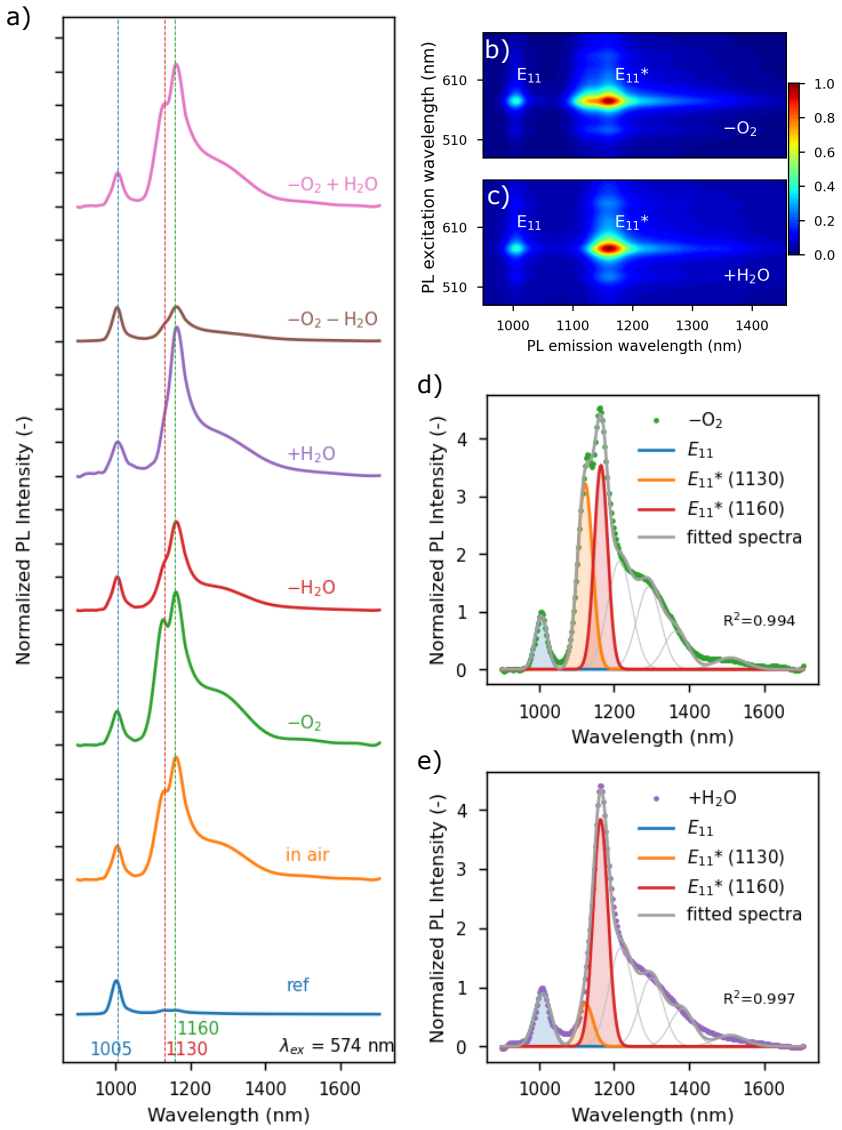

Figure 4.6. a) Normalized PL spectra of (6,5) SWCNTs functionalized with 3.8 mM BPO at 100°C under various conditions. The wavelengths at which the main peaks were found (E_{11} – 1005 nm, E_{11}* – 1130 nm and 1160 nm) are marked with dashed lines. PL excitation-emission maps of the samples prepared with b) argon and c) addition of water. PL spectra of the samples prepared with d) argon and e) addition of water fitted with component peaks: E_{11}, E_{11}* consisting of two peaks at 1130 and 1160 nm, and $E_{11}{}^{2}$* peaks at 1285, 1330, and 1355 nm. Figure was copied from reference P2.

appearance of the emission at around 1130 nm was slightly promoted when the O_2 was removed. Knowing that carbon-based radicals are rapidly trapped by molecular oxygen and other reactive oxygen species,[129] it seems reasonable to associate this particular emission feature with the attachment of phenyl or benzyl radicals to the SWCNT walls.

On the other hand, the spectra were significantly influenced by water content – the appearance of E_{11}* peak at 1160 nm was boosted with the addition of H_2O. This may be related to the role of water as an effective source of hydrogen atom, which saturates the radical formed on the

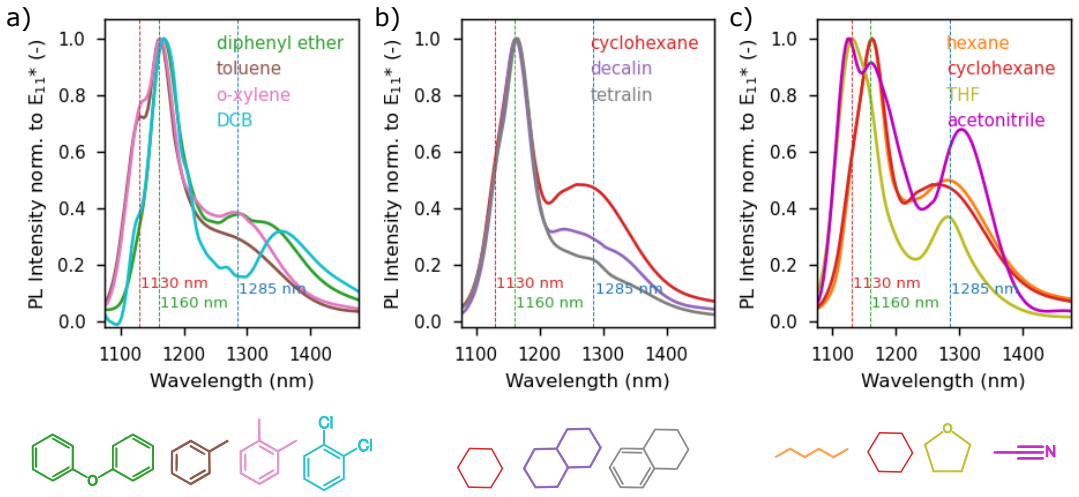

Figure 4.7. Comparison of defect emission spectra of (6,5) SWCNT functionalized with 3.8 mM BPO in mixed-solvent environments with chemical structure of the solvents used to dissolve BPO (co-solvents with toluene), shown below. Spectra are compared for a) diphenyl ether, toluene, o-xylene, and DCB, b) cyclohexane, decalin, and tetralin and c) hexane, cyclohexane, THF and acetonitrile co-solvents. Figure was copied from reference P2.

surface of SWCNTs after breaking a double bond and attachment of the aryl group.[128,130–133] Interestingly, the peak at 1130 nm was not prominent upon water addition nor removal, which made the functionalization reaction more selective. This was observed in PL maps (Figure 4.6b and c). Fitting PL spectra extracted from these maps allowed for the visualization of the particular peaks' contribution to PL emission (Figure 4.6d and e).

Due to the possibility of radical transfer to the solvent molecule, and creation of the secondary radicals leading to various defect configurations in the SWCNTs, the solvent selection is crucial for obtaining selective PL emission from modified SWCNTs. Additionally, the optical properties of the SWCNTs are sensitive to the microenvironment surrounding them, *e.g.* polymer conformation is altered in polar solvents. This was proven earlier for aqueous dispersions of the SWCNTs,[134] and corroborated here also for the organic ones. In general, polar and very non-polar solvents result with nanotubes precipitation, which prevents the PL measurements altogether. To better understand the role of liquid medium and its impact on the extent of functionalization, the reaction of SWCNTs with BPO was conducted in a 1:1 vol. mixture of toluene with another organic solvent, referred here as a co-solvent. Each mixed-solvent environment resulted with different shape of PL emission (Figure 4.7). They were not simply affected by the optical properties of the solvents themselves, nor by their dielectric constants. Instead, the results correlated with BPO decomposition reaction rates in the particular type of solvent in the employed temperature of 100 °C, and also with the solvent molecular structure. *E.g.* if the aromatic co-solvent molecule contained methyl groups (toluene, o-xylene), the carbon-based radicals were formed *via* the chain transfer reaction,[135] leading to the emission at 1130 nm wavelength (Figure 4.7a). This phenomenon was not observed in

case of tetralin (Figure 4.7b), probably due to presence of the aromatic rings. The aliphatic rings of cyclohexane and decalin led to high ratios of E_{11}*(1160)/E_{11}, due to high reaction rates of the solvent-induced unimolecular BPO decomposition, mentioned in the introduction. In case of these systems, limited emission at 1130 nm wavelength suggest low reactivity of the solvent-induced radicals with the SWCNTs. In case of cyclohexane and hexane (Figure 4.7c), additional further red-shifted emission in 1200-1450 nm range probably originated from the bimolecular functionalization, meaning the attachment of two benzoyloxy, or one benzoyloxy and one solvent-induced radical. The latter moieties reactivity towards the nanotubes depends on the radicals flexibility and size. When THF or acetonitrile was used as a co-solvent, the peak at 1130 nm wavelength was dominating in the obtained spectra, and the further red-shifted emission $>$1200 nm was also present. It can be explained by high decomposition reaction rates of BPO in these solvents and formation of the alternative, small radical structures (especially in case of acetonitrile) able to graft the SWCNTs.

To confirm that peak observed in spectra at 1130 nm originates from the C–C bond, the nanotubes were transferred to benzene and chlorobenzene, which does not contain any methyl groups. As expected, functionalization in these environments did not show emission at 1130 nm, even at high concentration (15 mM) of the BPO. Last but not least, the C–O bond, contrary to the C–C bond was prone to hydrolysis conducted using tetramethylammonium hydroxide (TMAH), which further corroborated the results.

This study allowed to further understand the mechanism of SWCNT functionalization for the purposes of PL emission, especially in terms of spectral selectivity. It showed, that upon proper selection of the temperature, solvent and environmental conditions, quick, effective and selective functionalization can be conducted using the BPO in organic environment, increasing the application potential of the SWCNTs in photonics.

4.3. BPO derivatives as a toolset for modifying PL emission from the SWCNTs

In this chapter and in publication **P3**, the focus was on gaining deeper insight into the radical chemistry of benzoyl peroxide (BPO) and its potential to enhance the photoluminescence (PL) emission of SWCNTs. For example, while BPO enabled the introduction of luminescent defects into the structure of (6,5) SWCNTs, it was found to be less effective for the larger-diameter (7,5) chirality (Table 3.2), which exhibits reduced reactivity due to lower curvature. Effective functionalization strategies for larger-diameter SWCNTs are nevertheless highly desirable, as these nanotubes exhibit a greater redshift in their optical emission. Moreover, even for small-diameter (6,5) SWCNTs, relatively high initiator concentrations at elevated reaction temperatures were required to achieve a satisfactory degree of functionalization. The underlying hypothesis of this study was that structural modification of the initiator could alter the reactivity of the resulting radical species toward SWCNTs of different chiralities, while also providing significantly improved control over physicochemical properties such as solubility, decomposition rate, and chemical stability.[117,136,137] The ability to tailor the chemical structure of BPO derivatives thus enables a more comprehensive understanding of the complex behavior associated with radical-based transformations and facilitates the identification of potential applications of this widely used class of compounds.

The reactivity of the BPO was tailored by the addition of functional groups. Commercial availability of these aryl peroxides is very limited, so they were synthesized in-house by the authors colleagues. Briefly, to get desired acyl peroxide, the acyl chloride was *in situ* transformed into peroxy acid in reaction with hydrogen peroxide and coupled with unreacted acyl chloride in presence of sodium hydroxide (Figure 4.8a). More details regarding this synthesis can be found in publication **P3** and Supporting Information. The procedure was implemented to provide series of BPO derivatives with alkyl, alkoxyl, carbonyl, halide, nitrile and nitro functional groups symmetrically attached to phenyl moiety (Figure 4.8b). Obtained peroxides were tested by me for functionalization of the (6,5) SWCNTs. Based on the results obtained, I used more reactive derivatives to functionalize also the (7,5) SWCNTs. The formation of C–O and C–C bonds at the SWCNTs surface, caused by the attachment of benzoyloxy and carbon-type radicals (Figure 4.8c), was observed in PL emission maps and spectra. Variations in the chemical structure of the initiator significantly affected both, the radical generation and their affinity towards the nanotubes. More electron-donating substituents (with lower values of Hammett constant σ) in the aryl peroxide structure made it less reactive, meaning that higher relative concentrations [R-BPO]/[CNT] and/or higher reaction temperature were necessary to obtain similar defect densities, measured by E_{11}*/E_{11} peak area ratios. Please notice, that this order is reversed comparing to the rate of spontaneous thermal decomposition of the substituted peroxide, meaning that the active nature of the substituent, which assures

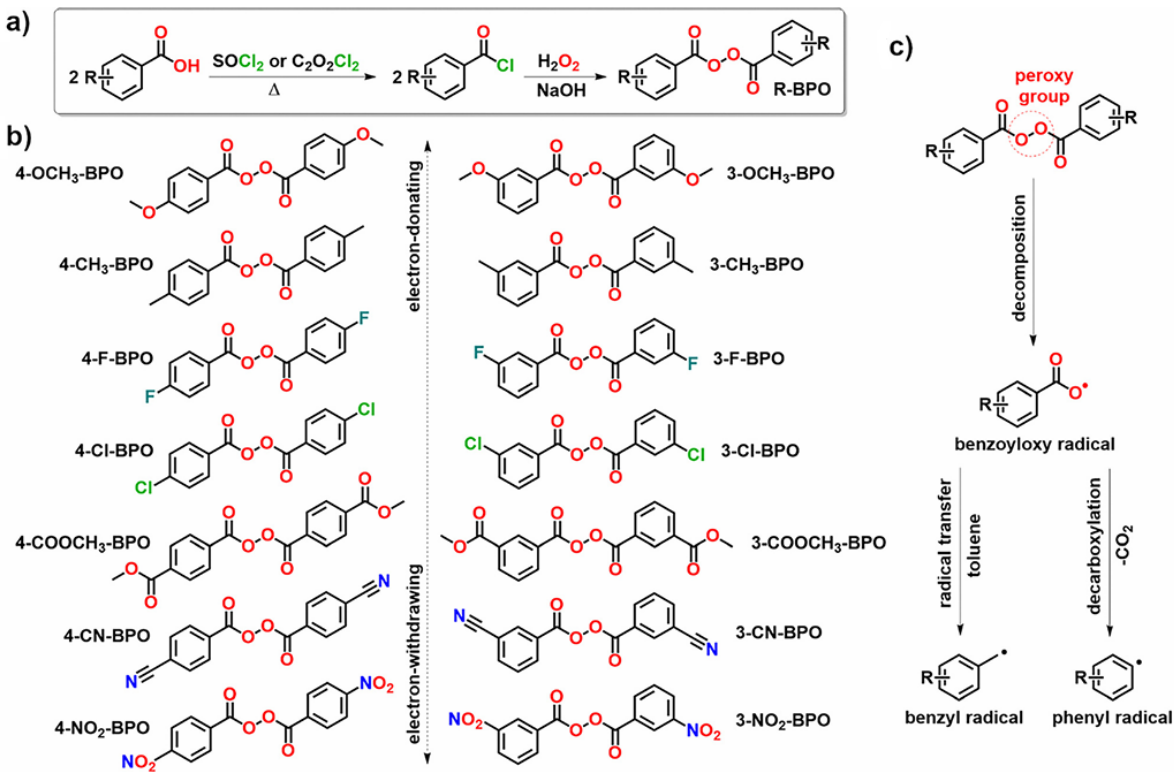

Figure 4.8. a) Synthetic approach used to obtain BPO derivatives. b) A spectrum of BPO derivatives produced for SWCNT functionalization. c) Decomposition of BPO derivatives giving rise to the generation of alternative carbon-type radicals for SWCNT functionalization. Figure was copied from reference P3.

the creation of functionalizing radicals, does not necessarily assure functionalization of the SWCNTs.

The electron density distribution which influences the reactivity is reflected in the Atom-Centered Charge (ACC) on the carbon atom adjacent to the carbonyl group (Figure 4.9a). For example, for the 4-CH_3-BPO reactant, the partial positive charge of 0.062 is slightly lower than for 3-CH_3-BPO (0.068) and unsubstituted BPO (0.067), which correlates with the increase in defect density under the influence of these compounds (Figure 4.9b-e). The correlation of the ACC with radical affinity towards the (6,5) SWCNTs was especially significant, when 4-OCH_3-BPO was used. The partial positive charge on the carbon atom adjacent to the carbonyl group was the lowest among tested (0.046) and this compound was found unable to functionalize the (6,5) SWCNTs in any conditions, even though the radicals were generated.

The same as for BPO, at high initiator excess, functionalization reaction accelerated, judging by the elevated E_{11}^*/E_{11} area ratios. The peak at *ca.* 1130 nm emerged for 4-CH_3-BPO and unsubstituted BPO, but also for the 3-OCH_3-BPO (Figure 4.10a). It was explained by the increased concentration of the benzyl radicals in the reaction mixture. Rate of decarboxylation of aryloxyl radicals, yielding secondary phenyl radicals, increases along the series 4-F-Ph-COO· $\leq$ 4-OCH_3-Ph-COO· $<$ 4-CH_3-Ph-COO· $\approx$ 4-Cl-Ph-COO· $<$ PhCOO· $<$ 3-Cl-Ph-COO·.[138]

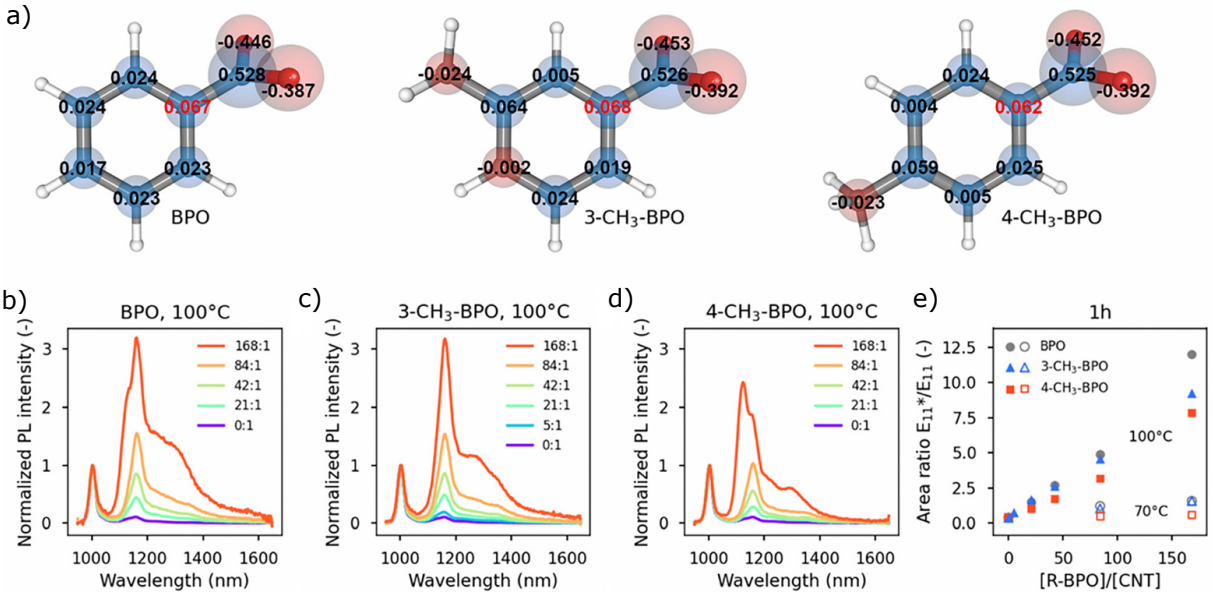

Figure 4.9. a) Calculated Atom Centered Charges for radicals derived from unsubstituted BPO, 3-CH_3-BPO, and 4-CH_3-BPO. b-d) PL spectra of SWCNTs functionalized using (b) unsubstituted, (c) 3-CH_3- and (d) 4-CH_3- substituted BPO in 1 hour-long reaction at 100 °C. e) The area ratios of E_{11}*/E_{11} peaks versus [R-BPO]/[CNT] concentration ratios. For better visibility, values obtained using 3- and 4-substituted BPOs were plotted using triangles and squares, respectively. Figure was copied from reference P3.

The reduced electrophilicity of the 4-CH_3-PhCOO· radical – arising from its electron-rich character – extends its lifetime because it is less prone to functionalize SWCNTs. This also increases the likelihood of radical transfer to the solvent (toluene). Consequently, phenyl radicals can convert into more stable benzyl radicals via the cage effect, in which surrounding solvent molecules transiently confine reactive intermediates and alter their reaction pathways, yielding the more stable species.[139]

Ester groups, connected *via* their carbonyl carbon, exert a strong electron withdrawing behavior due to combination of the $-I$ and $-R$ effects. Analysis of optical spectra collected at 100 °C revealed clear differences in both reactivity and the resulting spectral features between methoxy- and ester-substituted peroxides, as well as the effect of functional group position. While 3-$COOCH_3$-BPO showed a distinct additional peak at *ca.* 1300 nm, 4-$COOCH_3$-BPO exhibited no notable features beyond the primary E_{11}* defect at 1166 nm. Moreover, using both 3-$COOCH_3$ and 3-OCH_3 for SWCNT functionalization led to a pronounced increase in the *ca.* 1300 nm peak compared to spectra from unsubstituted BPO. This was attributed to the interactions between 3-position substituents and the SWCNT sidewall, consistent with Yu *et al.*, who reported that similar *meta*-substituted modifications of SWCNTs produce strongly redshifted PL peaks.[140] Such specific interactions – particularly strong for reactive *meta* substituents – can promote localized defect clustering and, at higher concentrations, result

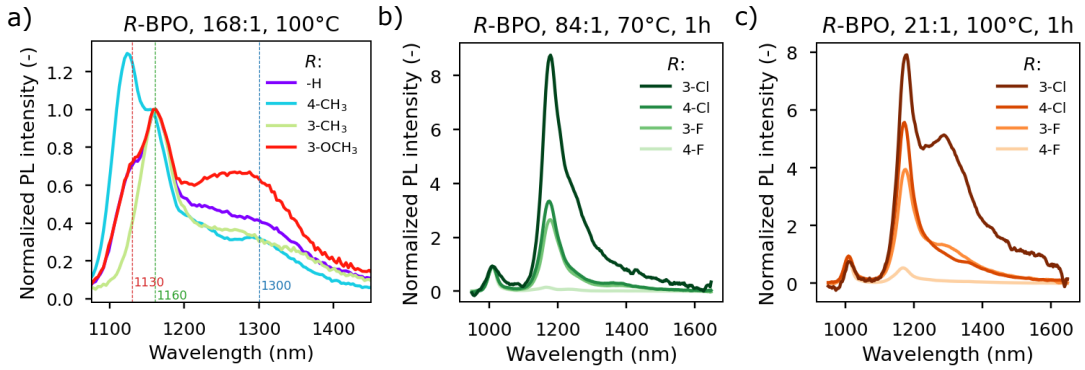

Figure 4.10. a) Comparison of spectral shapes of the defect region E_{11}*, especially the E_{11}*(1130) peak, obtained with large excess of different initiators. Comparison of PL spectra obtained with halogen-substituted BPO, at (e) lower temperature but higher [R-BPO]/[CNT] and (f) higher temperature but lower [R-BPO]/[CNT]. Figure was copied from reference P3.

in overfunctionalization and fluorescence quenching, observed as increased noise and light scattering in the PL spectra (further discussed in the SI).

Halogen substituted BPO (F-BPO and Cl-BPO) also exerted significantly different electronic effects depending on the functional group position. Again, more electron-withdrawing *meta*-substituted structures were proven more reactive and for high initiator concentrations the formation of far redshifted peak at *ca.* 1300 nm was observed (Figure 4.10b and c). Width of this fluorescent emission band was increasing with the substituent group size. Interestingly, the band located at *ca.* 1130 nm, corresponding to carbon-type radicals on the surface of the SWCNT, was not observed in any case.

Finally, strongly electron-withdrawing nitro- and cyano- groups were introduced into the BPO structure. Especially electron-poor *para*-substituted counterparts were weakly soluble in toluene. They required high [R-BPO]/[CNT] concentration ratios to successfully functionalize the (6,5) SWCNTs. On the contrary, nitrogen-containing substituents in the 3− position led to extreme reactivity towards the (6,5) SWCNTs, allowing for substantial decrease of the [R-BPO]/[CNT] concentration ratio and/or reaction temperature. For SWCNTs exposed to higher concentrations of 3-NO_2-BPO, uncontrolled functionalization occurred, producing a jagged optical spectrum and, eventually, complete fluorescence quenching. This behavior supported previous findings that SWCNT functionalization may become self-accelerating, when reactant molecules are abundant.[141] This is because adding new functional groups becomes energetically more favorable on an already modified surface. Consequently, multiple defects can accumulate in the affected region, degrading the optical properties of SWCNTs. Thus, it is essential to optimize the functionalization conditions so that reactive radicals are fully consumed during the process or deactivated using radical scavengers. This was discussed in greater details in the Supporting Information for publication **P3**.

To further prove, that the electron-poor substituent in the initiator structure lead to increased

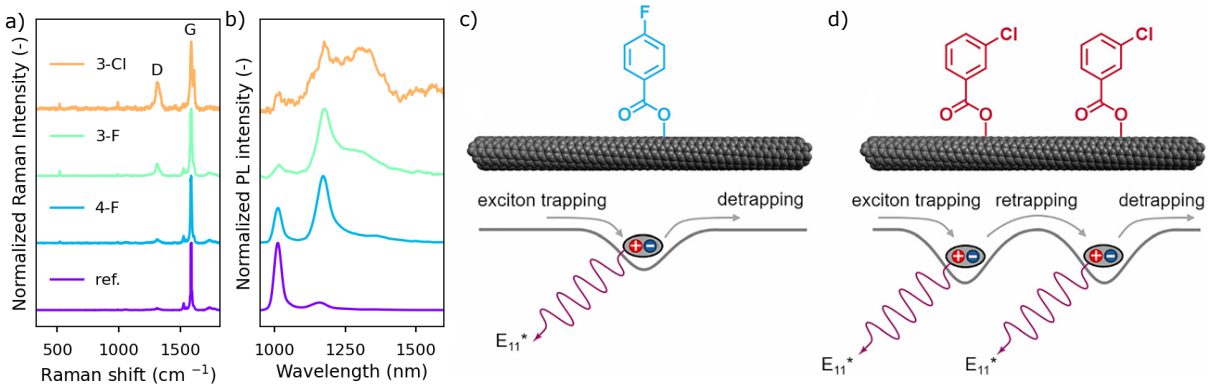

Figure 4.11. a) Raman spectra of pristine SWCNTs and modified with 3-Cl-BPO, 3-F-BPO, and 4-F-BPO. Excitation wavelength was 532 nm. b) Corresponding PL spectra normalized to the intensity of the maximum of the peak of the highest intensity obtained upon excitation at 574 nm. SWCNT reacted with c) 4-F-BPO, and d) 3-Cl-BPO with the schematics of the main phenomena related to exciton dynamics in SWCNTs modified with luminescent defects. Figure was copied from reference P3.

defect density on the SWCNTs' surfaces, the PL emission spectra were correlated with Raman spectra. For this experiment, the (6,5) SWCNTs were functionalized in identical conditions but with different radical initiators: 4-F-, 3-F- and 3-Cl-BPO (4.11a and b). The observed increase in the intensity ratio of the D to G bands in the Raman spectra confirmed more severe modification for more electron-withdrawing substituents in BPO structure. It was proposed, that the introduced exciton traps are not only deeper, as previously disclosed,[17] but the underlying photophysics was also changed. For these SWCNTs, which are supposedly more functionalized, it is likely that excitons, which generally have high mobility[142,143] can be detrapped and effectively retrapped by the defect sites present in abundance (Figure 4.11c and d). Radiative recombination becomes therefore much probable, explaining stronger E_{11}* spectral features. Similar phenomena were recently described by Sebastian *et al.*[144] in case of oxygen-based defects.

Increasing electron deficiency of the functionalizing group was earlier proved to redshift the E_{11}* emission from the diazonium-functionalized SWCNTs.[71] BPO derivatives exhibit similar effect, although here several groups of values were observed (Figure 4.12). Within each group, substituents with significantly different Hammett σ values lead to similar E_{11}* redshifts, *e.g.* 4-CH_3, 3-CH_3, -H, 4-F, 3-OCH_3 or 4-Cl, 3-F, 3-$COOCH_3$ or 3-NO_2, 4-NO_2, 4-CN. Also significant differences were observed for a given substituent in 4- or 3- position. They could arise from steric effects, variations in the spatial arrangement or orientation of the attached functional group relative to the SWCNT surface, or subtle changes in the electronic coupling between the substituent and the SWCNT lattice, depending on the *meta-* or *para-* orientation.

Various reactivity of the BPO substituents towards the (6,5) SWCNTs is a powerful tool for covalent functionalization of other chiralities. Larger SWCNTs have further redshifted emission, which could enable operation in the telecommunication window. However, they are

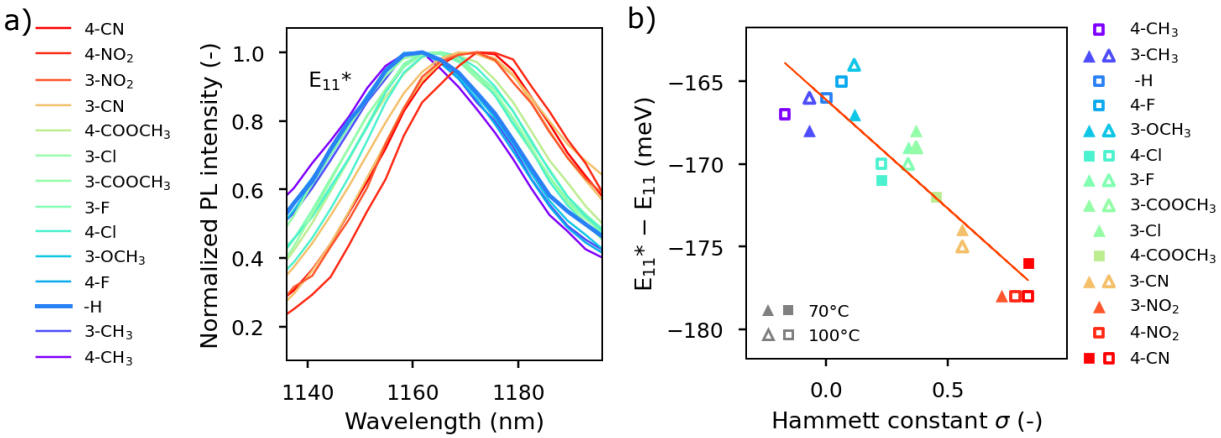

Figure 4.12. a) Normalized E_{11}* peaks of (6,5) SWCNTs obtained upon functionalization using benzoyloxyl radicals with different substituents. Line colors were selected in linear dependence on the Hammet substituent constant. b) Close to the linear dependence of the experimentally observed optical trap depth on the Hammett constant. For better visibility, values obtained using 3- and 4-substituted BPOs were plotted using triangles and squares, respectively. Figure was copied from reference P3.

also known to be substantially less reactive, due to reduced curvature.[145,146] The (7,5) SWCNTs were not prone to functionalization using unsubstituted BPO, but it successfully functionalized using 5 more reactive derivatives, *i.e.* 4-$COOCH_3$-, 4-Cl-, 3-Cl-, 3-CN- and 3-NO_2-BPO.

The systematic investigation presented in this work, supported by detailed kinetic studies and analysis of substituent effects, offers valuable insight into the surface chemistry of SWCNTs, enabling more rational design of nanomaterials for optoelectronic applications. In addition, the library of in-house–synthesized BPO derivatives reveals how structural modification can tune their electrophilicity and, in turn, the efficiency of key chemical transformations.

5. Conclusions

This study expands previous understanding of mechanisms underlying the reactivity of the SWCNTs, in the context of both chirally selective isolation using polyfluorenes and radical initiated covalent functionalization. Both processes are scalable and require only common equipment and operators' skills, which makes them promising in terms of applications. In the same time they allow to observe an abundance of fascinating physicochemical phenomena.

Affinity of the CP towards the small diameter SWCNTs of specific chiralities was known to be highly dependent on the chain length, but here the consequences of this fact for the recurrent extraction process were elucidated. The highest extraction yields reported so far were obtained here, when temperature, sonication time and power were adjusted to the polymer macromolecular parameters, *i.e.* higher temperature and sonication time improved the isolation yield especially for CPs of high molecular weight. On the other hand, higher excess of the CP over SWCNTs could enable successful isolation using short-chained re-cycled polymer material. This knowledge enables more effective using of the existing CPs and allows to better predict the desired properties of the ones dedicated for the nanotubes extraction in the future. Additionally, the CPE process enabled use of a different solvent without significant changes in the procedure, as long as the new solvent was structurally similar and assured the CP solubility.

In laboratory practice, these observations were extremely useful to obtain dispersions of the (6,5) and (7,5) SWCNTs in toluene, having great potential for modern thin-film optical devices. Compatible methods of precise tuning of the PL emission from these materials were developed here, demonstrating the potential of well known radical reagent, *i.e.* BPO and its derivatives. Optimal conditions for the reaction of controlled defect implantation included moderate level of temperature (70–85°C), low radical initiator concentration and proper combination of the solvent and radical structures. Please notice, that *e.g.* decarboxylation of the benzoyloxy radicals could be reduced either by using solvents containing no methyl groups or electron-withdrawing substituents to BPO. Importantly, the substituents in radical initiator structure modified not only the exciton trap depth, as it was shown in earlier studies, but also directly influenced the reactivity of the created radicals toward the SWCNTs, which allowed *e.g.* for successful functionalization of the larger (7,5) SWCNTs.

In summary, this research provides a comprehensive understanding of the process of SWCNT functionalization, offering a new approach into controlled engineering of the luminescent defects and can be useful for rational designing of the processes and materials for new optoelectronic applications.

Bibliography

[1] R. Feynman. There's plenty of room at the bottom. *Eng. Sci.*, 23(5):22–36, 1960.

[2] L.V. Radushkevich and V.M. Lukyanovich. O strukture ugleroda, obrazujucegosja pri termiceskom razlozenii okisi ugleroda na zeleznom kontakte. *Russ. J. Phys. Chem.*, 26:88–95, 1952.

[3] K. Nishiyama, S. Miura, and K. Katada. Crystal growth of GaN by the reaction of Ga with NH_3. *Journal of Crystal Growth*, 33(3):334–339, 1976.

[4] S. Iijima. Helical microtubules of graphitic carbon. *Nature*, 354(6348):56–58, 1991.

[5] S. Hong and S. Myung. A flexible approach to mobility. *Nature Nanotechnology*, 2:207–208, 2007.

[6] G. J. Brady, A. J. Way, N. S. Safron, H. T. Evensen, P. Gopalan, and M. S. Arnold. Quasi-ballistic carbon nanotube array transistors with current density exceeding Si and GaAs. *Sci. Adv.*, 2(9):e1601240, 2016.

[7] L. Yu, C. Shearer, and J. Shapter. Recent development of carbon nanotube transparent conductive films. *Chem. Rev.*, 116(22):13413–13453, 2016.

[8] K.K. Koziol, D. Janas, E. Brown, and L. Hao. Thermal properties of continuously spun carbon nanotube fibres. *Phys. E*, 88:104–108, 2017.

[9] Z. Han and A. Fina. Thermal conductivity of carbon nanotubes and their polymer nanocomposites: A review. *Prog. Polym. Sci.*, 36(7):914–944, 2011.

[10] M.F. Yu, O. Lourie, M. J. Dyer, K. Moloni, T. F. Kelly, and R. S. Ruoff. Strength and breaking mechanism of multi walled carbon nanotubes under tensile load. *Science*, 287(5453):637–640, 2000.

[11] M.M.J. Treacy, T. W. Ebbesen, and J. M. Gibson. Exceptionally high Young's modulus observed for individual carbon nanotubes. *Nature*, 381(6584):678–680, 1996.

[12] Y. Matsuda, J. Tahir-Kheli, and W. A. Goddard III. Definitive band gaps for single-wall carbon nanotubes. *J. Phys. Chem. Lett.*, 1(19):2946–2950, 2010.

[13] J.W. Mintmire and C.T. White. Universal density of states for carbon nanotubes. *Phys. Rev. Lett.*, 81(12):2506–2509, 1998.

[14] C.T. White, D.H. Robertson, and J.W. Mintmire. Helical and rotational symmetries of nanoscale graphitic tubules. *Phys. Rev. B*, 47(9):5485–5488, 1993.

[15] C. T. White and J. W. Mintmire. Fundamental properties of single-wall carbon nanotubes. *J. Phys. Chem. B*, 109(1):52–65, 2005.

[16] M. J. O'Connell, S. M. Bachilo, C. B. Huffman, V. C. Moore, M. S. Strano, E. H. Haroz, K. L. Rialon, P. J. Boul, W. H. Noon, C. Kittrell, J. Ma, R. H. Hauge, R. B. Weisman, and R. E. Smalley. Band gap fluorescence from individual single-walled carbon nanotubes. *Science*, 297(5581):593–596, 2002.

[17] J. Zaumseil. Luminescent defects in single-walled carbon nanotubes for applications. *Adv. Optical Mater.*, 10(2):2101576, 2022.

[18] J. Crochet, M. Clemens, and T. Hertel. Quantum yield heterogeneities of aqueous single-wall carbon nanotube suspensions. *J. Am. Chem. Soc.*, 129(26):8058–8059, 2007.

[19] A.C. Dupuis. The catalyst in the CCVD of carbon nanotubes – a review. *Prog. Mater. Sci.*, 50(8):929–961, 2005.

[20] V. Jourdain and C. Bichara. Current understanding of the growth of carbon nanotubes in catalytic chemical vapour deposition. *Carbon*, 58:2–39, 2013.

[21] K.A. Shah and B.A. Tali. Synthesis of carbon nanotubes by catalytic chemical vapour deposition: A review on carbon sources, catalysts and substrates. *Mater. Sci. Semicond. Process.*, 41:67–82, 2016.

[22] J. Chrzanowska, J. Hoffman, A. Małolepszy, M. Mazurkiewicz, T.A. Kowalewski, Z. Szymański, and L. Stobiński. Synthesis of carbon nanotubes by the laser ablation method: Effect of laser wavelength. *Phys. Status Solidi B*, 252(8):1860–1867, 2015.

[23] A. Meyer-Plath, G. Orts-Gil, S. Petrov, F. Oleszak, H.-E. Maneck, I. Dörfel, O. Haase, S. Richter, and R. Mach. Plasma-thermal purification and annealing of carbon nanotubes. *Carbon*, 50(10):3705–3714, 2012.

[24] N. Arora and N.N. Sharma. Arc discharge synthesis of carbon nanotubes: Comprehensive review. *Diam. Relat. Mat.*, 50:135–150, 2014.

[25] I.W. Chiang, B.E. Brinson, A.Y. Huang, P.A. Willis, M.J. Bronikowski, J.L. Margrave, R.E. Smalley, and R.H. Hauge. Purification and characterization of single-wall carbon nanotubes (SWNTs) obtained from the gas-phase decomposition of CO (HiPco process). *J. Phys. Chem. B*, 105:8297–8301, 2001.

[26] S.M. Bachilo, L. Balzano, J.E. Herrera, F. Pompeo, D.E. Resasco, and R.B. Weisman. Narrow (n,m)-distribution of single-walled carbon nanotubes grown using a solid supported catalyst. *J. Am. Chem. Soc.*, 125(37):11186–11187, 2003.

[27] M.R. Predtechenskiy, A.A. Khasin, A.E. Bezrodny, O.F. Bobrenok, D.Y. Dubov, V.E. Muradyan, V.O. Saik, and S.N. Smirnov. New perspectives in SWCNT applications: Tuball SWCNTs. Part 1. Tuball by itself — all you need to know about it. *Carbon Trends*, 8:100175, 2022.

[28] D. Janas. Towards monochiral carbon nanotubes: a review of progress in the sorting of single-walled carbon nanotubes. *Mater. Chem. Front.*, 2(1):36–63, 2018.

[29] A. Nish and R.J. Nicholas. Temperature induced restoration of fluorescence from oxidised single-walled carbon nanotubes in aqueous sodium dodecylsulfate solution. *Phys. Chem. Chem. Phys.*, 8:3547–3551, 2006.

[30] O. Matarredona, H. Rhoads, Z. Li, J. H. Harwell, L. Balzano, and D.E. Resasco. Dispersion of single-walled carbon nanotubes in aqueous solutions of the anionic surfactant NaDDBS. *J. Phys. Chem. B*, 107(48):13357–13367, 2003.

[31] B.S. Flavel, K.L. Moore, S.H. Tolbert, A.G. Guthy, A.C. Lau, S.K. Doorn, R.H. Hauge, J. Kono, B.G. Iglehart, M.E. Shahidi, R.H. Yong, V. Kis, C.M. Hébert, P.M. Ajayan, B.M. Weaver, A.M. Mukherjee, M.H. Davis, K.E. Gates, T.S. Benz, and J.M. Scarpulla. Separation of single-walled carbon nanotubes with a gel permeation chromatography system. *ACS Nano*, 8(2):1817–1826, 2014.

[32] J.W.T. Seo, N.L. Yoder, T.A. Shastry, J.J. Humes, J.E. Johns, A.A. Green, and M.C. Hersam. Diameter refinement of semiconducting arc discharge single-walled carbon nanotubes via density gradient ultracentrifugation. *J. Phys. Chem. Lett.*, 4(17):2805–2810, 2013.

[33] N.K. Subbaiyan, S. Cambré, A.N.G. Parra-Vasquez, E.H. Hároz, S.K. Doorn, and J.G. Duque. Role of surfactants and salt in aqueous two-phase separation of carbon nanotubes toward simple chirality isolation. *ACS Nano*, 8(2):1619–1628, 2014.

[34] D. Fong and A. Adronov. Recent developments in the selective dispersion of single-walled carbon nanotubes using conjugated polymers. *Chem. Sci.*, 8:7292–7305, 2017.

[35] J. Wang and T. Lei. Separation of semiconducting carbon nanotubes using conjugated polymer wrapping. *Polymers*, 12(7):1548, 2020.

[36] J. Ding, Z. Li, J. Lefebvre, F. Cheng, G. Dubey, S. Zou, P. Finnie, A. Hrdina, L. Scoles, G.P. Lopinski, C.T. Kingston, B. Simard, and P.R.L. Malenfant. Enrichment of large-diameter semiconducting SWCNTs by polyfluorene extraction for high network density thin film transistors. *Nanoscale*, 6:2328–2339, 2014.

[37] J. Lefebvre, J. Ding, Z. Li, P. Finnie, G. Lopinski, and P.R.L. Malenfant. High-purity semiconducting single-walled carbon nanotubes: A key enabling material in emerging electronics. *Acc. Chem. Res.*, 50(10):2479–2486, 2017.

[38] F. Chen, B. Wang, Y. Chen, and L.-J. Li. Toward the extraction of single species of single-walled carbon nanotubes using fluorene-based polymers. *Nano Lett.*, 7(10):3013–3017, 2007.

[39] A. Graf, Y.E. Zakharko, S.P. Schießl, C. Backes, M. Pfohl, B.S. Flavel, and J. Zaumseil. Large scale, selective dispersion of long single-walled carbon nanotubes with high photoluminescence quantum yield by shear force mixing. *Carbon*, 105(593):593–599, 2016.

[40] A. Dzienia, D. Just, P. Taborowska, A. Mielanczyk, K.Z. Milowska, S. Yorozuya, S. Naka, T. Shiraki, and D. Janas. Mixed-solvent engineering as a way around the trade-off between yield and purity of (7,3) single-walled carbon nanotubes obtained using conjugated polymer extraction. *Small*, 19(46):2304211, 2023.

[41] L. Xu, M. Valášek, F. Hennrich, E. Sedghamiz, M. Penaloza-Amion, D. Häussinger, W. Wenzel, M.M. Kappes, and M. Mayor. Enantiomeric separation of semiconducting single-walled carbon nanotubes by acid cleavable chiral polyfluorene. *ACS Nano*, 15(3):4699–4709, 2021.

[42] W. Gomulya, G.D. Costanzo, E.J. Figueiredo de Carvalho, S.Z. Bisri, V. Derenskyi, M. Fritsch, N. Fröhlich, S. Allard, P. Gordiichuk, A. Herrmann, S.J. Marrink, M.C. dos Santos, U. Scherf, and M.A. Loi. Semiconducting single-walled carbon nanotubes on demand by polymer wrapping. *Adv. Mater.*, 25(21):2948–2956, 2013.

[43] J. Ouyang, J. Ding, J. Lefebvre, Z. Li, C. Guo, A.J. Kell, and P.R.L. Malenfant. Sorting of semiconducting single-walled carbon nanotubes in polar solvents with an amphiphilic conjugated polymer provides general guidelines for enrichment. *ACS Nano*, 12:1910–1919, 2018.

[44] A. Nish, J.-Y. Wang, J. Doig, and R.J. Nicolas. Highly selective dispersion of single walled carbon nanotubes using aromatic polymers. *Nat. Nanotech.*, 2:640–646, 2007.

[45] D. Ji, S. Kim, M. Han, S. Jeon, B. Lim, and Y.-Y. Noh. One-step sorting of nearly single-chiral carbon nanotubes with (10,9) chirality of 1.3 nm diameter by backbone planarization of polydioctylfluorenes. *Carbon*, 219:118791, 2024.

[46] H. Ozawa, N. Ide, T. Fujigaya, Y. Niidome, and N. Nakashima. One-pot separation of highly enriched (6,5)-single-walled carbon nanotubes using a fluorene-based copolymer. *Chem. Lett.*, 40(3):239–241, 2011.

[47] F. Jakubka, S.P. Schiessl, S. Martin, J.M. Englert, F. Hauke, A. Hirsch, and J. Zaumseil. Effect of polymer molecular weight and solution parameters on selective dispersion of single-walled carbon nanotubes. *ACS Macro Lett.*, 1(7):815–819, 2012.

[48] Y. Joo, G.J. Brady, M.J. Shea, M.B. Oviedo, C. Kanimozhi, S.K. Schmitt, B.M. Wong, M.S. Arnold, and P. Gopalan. Isolation of pristine electronics grade semiconducting carbon nanotubes by switching the rigidity of the wrapping polymer backbone on demand. *ACS Nano*, 9(10):10203–10213, 2015.

[49] H. Wang, G.I. Koleilat, P. Liu, G. Jiménez-Osés, Y.-C. Lai, M. Vosgueritchian, Y. Fang, S. Park, K.N. Houk, and Z. Bao. Correction to high-yield sorting of small-diameter carbon nanotubes for solar cells and transistors. *ACS Nano*, 8(7):6511–7550, 2014.

[50] S.K. Samanta, M. Fritsch, U. Scherf, W. Gomulya, S.Z. Bisri, and M.A. Loi. Conjugated polymer-assisted dispersion of single-wall carbon nanotubes: The power of polymer wrapping. *ACC Chem. Res.*, 47(8):2446–2456, 2014.

[51] N. Berton, F. Lemasson, F. Hennrich, M.M. Kappes, and M. Mayor. Influence of molecular weight on selective oligomer-assisted dispersion of single-walled carbon nanotubes and subsequent polymer exchange. *Chem. Commun*, 48:2516–2518, 2012.

[52] A. Dzienia, D. Just, T. Wasiak, K.Z. Milowska, A. Mielanczyk, N. Labedzki, S. Kruss, and D. Janas. Size matters in conjugated polymer chirality-selective SWCNT extraction. *Adv. Sci.*, 11(29):2402176, 2024.

[53] J. Ouyang, H. Shin, P. Finnie, J. Ding, C. Guo, Z. Li, Y. Chen, L. Wei, A. J. Wu, S. Moisa, F. Lapointe, and P.R.L. Malenfant. Impact of conjugated polymer characteristics on the enrichment of single-chirality single-walled carbon nanotubes. *ACS Appl. Polym. Mater.*, 4(8):6239–6254, 2022.

[54] R. Si, L. Wei, H. Wang, D. Su, S.H. Mushrif, and Y. Chen. Extraction of (9,8) single-walled carbon nanotubes by fluorene-based polymers. *Chem. Asian J.*, 9:868–877, 2014.

[55] N.A. Rice, A.V. Subrahmanyam, S.E. Laengert, and A. Adronov. The effect of molecular weight on the separation of semiconducting single-walled carbon nanotubes using poly(2,7-carbazole)s. *J. Polym. Sci. A: Polym. Chem.*, 53(21):2510–2516, 2015.

[56] H. Zhu, L. Hong, H. Tanaka, X. Ma, and C. Yang. Facile solvent mixing strategy for extracting highly enriched (6,5) single-walled carbon nanotubes in improved yield. *Bull. Chem. Soc. Jpn.*, 94(4):1166–1171, 2021.

[57] F. Liu, X. Chen, H. Liu, J. Zhao, M. Xi, H. Xiao, T. K. Lu, Y. Cao, Y. Li, L. Peng, and X. Liang. High-yield and low-cost separation of high-purity semiconducting single-walled carbon nanotubes with closed-loop recycling of raw materials and solvents. *Nano Res.*, 14(11):4281–4287, 2021.

[58] D. Just, A. Dzienia, K.Z. Milowska, A. Mielańczyk, and D. Janas. High-yield and chirality-selective isolation of single-walled carbon nanotubes using conjugated polymers and small molecular chaperones. *Mater. Horiz.*, 11:758–767, 2024.

[59] T. Schuettfort, H. J. Snaith, A. Nish, and R.J. Nicholas. Synthesis and spectroscopic characterization of solution-processable highly ordered polythiophene–carbon nanotube nanohybrid structures. *Nanotechnology*, 21(2):025201, 2010.

[60] Y. Joo, G.J. Brady, C. Kanimozhi, J. Ko, M.J. Shea, M.T. Strand, M.S. Arnold, and P. Gopalan.

Polymer-free electronic-grade aligned semiconducting carbon nanotube array. *ACS Appl. Mater. Interfaces*, 9(34):28859–28867, 2017.

[61] F.J. Berger, J. Lüttgens, T. Nowack, T. Kutsch, S. Lindenthal, L. Kistner C.C. Müller, L.M. Bongartz, V.A. Lumsargis, Y. Zakharko, and J. Zaumseil. Brightening of long, polymer-wrapped carbon nanotubes by sp^3 functionalization in organic solvents. *ACS Nano*, 13(8):9259–9269, 2019.

[62] W. Xu, M. Li, M. Tange, L. Li, J. Hou, J. Ye, L. Wei, Y. Chen, and J. W. Zhao. Printed thin film transistors with 10^8 On/Off ratios and photoelectrical synergistic characteristics using isoindigo-based polymers-enriched (9,8) carbon nanotubes. *Nano Res.*, 15(6):5517–5526, 2022.

[63] C.M. Homenick, R. James, G.P. Lopinski, J. Dunford, J. Sun, H. Park, Y. Jung, G. Cho, and P.R.L. Malenfant. Fully printed and encapsulated SWCNT-based thin film transistors via a combination of R2R gravure and inkjet printing. *ACS Appl. Mater. Interfaces*, 8(41):27900–27910, 2016.

[64] D.H. Arias, D.B. Sulas-Kern, S.M. Hart, H.S. Kang, J. Hao, R. Ihly, J.C. Johnson, J.L. Blackburn, and A.J. Ferguson. Effect of nanotube coupling on exciton transport in polymer-free monochiral semiconducting carbon nanotube networks. *Nanoscale*, 11(44):21196–21206, 2019.

[65] B. Mirka, N.A. Rice, P. Williams, M. N. Tousignant, N.T. Boileau, W.J. Bodnaryk, D. Fong, A. Adronov, and B.H. Lessard. Excess polymer in single-walled carbon nanotube thin-film transistors: Its removal prior to fabrication is unnecessary. *ACS Nano*, 15(5):8252–8266, 2021.

[66] M. Kim, X. Wu, G. Ao, X. He, H. Kwon, N. F. Hartmann, M. Zheng, S. K. Doorn, and Y. H. Wang. Mapping structure-property relationships of organic color centers. *Chem.*, 4(9):2180–2191, 2018.

[67] A.R. Amori, Z. Hou, and T.D. Krauss. Excitons in single-walled carbon nanotubes and their dynamics. *Annu. Rev. Phys. Chem.*, 69:81–99, 2018.

[68] G. Soavi, F. Scotognella, G. Lanzani, and G. Cerullo. Ultrafast photophysics of single-walled carbon nanotubes. *Adv. Opt. Mater.*, 4(11):1670–1688, 2016.

[69] N.F. Zorn and J. Zaumseil. Charge transport in semiconducting carbon nanotube networks. *Appl. Phys. Rev.*, 8(4):041318, 2021.

[70] A.H. Brozena, M. Kim, L.R. Powell, and Y. Wang. Controlling the optical properties of carbon nanotubes with organic colour-centre quantum defects. *Nat. Rev. Chem.*, 3:375–392, 2019.

[71] Y. Piao, B. Meany, L.R. Powell, N. Valley, H. Kwon, G.C. Schatz, and Y. Wang. Brightening of carbon nanotube photoluminescence through the incorporation of sp^3 defects. *Nature Chem.*, 5:840–845, 2013.

[72] S. Ghosh, S.M. Bachilo, R.A. Simonette, K.M. Beckingham, and R.B. Weisman. Oxygen doping modifies near-infrared band gaps in fluorescent single-walled carbon nanotubes. *Science*, 330(6011):1656–1659, 2010.

[73] H. Kwon, L.R. Powell, Y. Wang, S. Meany, Y. Piao, S.K. Doorn, S. Tretiak, and H. Htoon. Molecularly tunable fluorescent quantum defects in single-walled carbon nanotubes. *J. Am. Chem. Soc.*, 138(22):6974–6981, 2016.

[74] T. Shiraki, S. Uchimura, T. Shiraishi, H. Onitsuka, and N. Nakashima. Near infrared photoluminescence modulation by defect site design using aryl isomers in locally functionalized single-walled carbon nanotubes. *Chem. Commun.*, 53:12544–12547, 2017.

[75] B.J. Gifford, S. Tretiak, and S.K. Doorn. Optical effects of divalent functionalization of carbon nanotubes. *Chem. Mater.*, 31(17):6950–6959, 2019.

[76] B.J. Gifford, S. Kilina, H. Htoon, S.K. Doorn, and S. Tretiak. Exciton localization and optical emission in aryl-functionalized carbon nanotubes. *J. Phys. Chem. C*, 122(3):1828–1838, 2018.

[77] Y. Maeda, R. Morooka, P. Zhao, M. Yamada, and M. Ehara. Control of functionalized single-walled carbon nanotube photoluminescence via competition between thermal rearrangement and elimination. *Chem. Commun.*, 59:11648–11651, 2023.

[78] A. H. Brozena, J. D. Leeds, Y. Zhang, J. T. Fourkas, and Y. Wang. Controlled defects in semiconducting carbon nanotubes promote efficient generation and luminescence of trions. *ACS Nano*, 8(5):4239–4247, 2014.

[79] D. Janas. Perfectly imperfect: a review of chemical tools for exciton engineering in single-walled carbon nanotubes. *Mater. Horiz.*, 7:2860–2881, 2020.

[80] Y. Maeda, P. Zhao, and M. Ehara. Recent progress in controlling the photoluminescence properties of single-walled carbon nanotubes by oxidation and alkylation. *Chem. Commun.*, 59(98):14497–14508, 2023.

[81] T.J. McDonald, J.L. Blackburn, W.K. Metzger, G. Rumbles, and M.J. Heben. Chiral-selective protection of single-walled carbon nanotube photoluminescence by surfactant selection. *J. Phys. Chem. C*, 111(48):17894–17900, 2007.

[82] S. Settele, F. Stammer, F. L. Sebastian, S. Lindenthal, S.R. Wald, H. Li, B.S. Flavel, and J. Zaumseil. Easy access to bright oxygen defects in biocompatible single-walled carbon nanotubes via a Fenton-like reaction. *ACS Nano*, 18(31):20667–20678, 2024.

[83] X. Ma, L. Adamska, H. Yamaguchi, S.E. Yalcin, S. Tretiak, S.K. Doorn, and H. Htoon. Electronic structure and chemical nature of oxygen dopant states in carbon nanotubes. *ACS Nano*, 8(10):10782–10789, 2014.

[84] Y. Iizumi, M. Yudasaka, J. Kim, H. Sakakita, T. Takeuchi, and T. Okazaki. Oxygen-doped carbon nanotubes for near-infrared fluorescent labels and imaging probes. *Sci, Rep.*, 8:6272, 2018.

[85] C.-W. Lin, S.M. Bachilo, Y. Zheng, U. Tsedev, S. Huang, R.B. Weisman, and A.M. Belcher. Creating fluorescent quantum defects in carbon nanotubes using hypochlorite and light. *Nat. Commun.*, 10:2874, 2019.

[86] T. Eremin, V. Eremina, Y. Svirko, and P. Obraztsov. Over two-fold photoluminescence enhancement from single-walled carbon nanotubes induced by oxygen doping. *Nanomaterials*, 13(9):1561, 2023.

[87] C.F. Chiu, W.A. Saidi, V.E. Kagan, and A. Star. Defect-induced near-infrared photoluminescence of single-walled carbon nanotubes treated with polyunsaturated fatty acids. *J. Am. Chem. Soc.*, 139(13):4859–4865, 2017.

[88] Y. Niidome, R. Hamano, K. Nakamura, S. Qi, S. Ito, B. Yu, Y. Nagai, N. Tanaka, T. Mori, Y. Katayama, T. Fujigaya, and T. Shiraki. Near-infrared photoluminescent detection of serum albumin using single-walled carbon nanotubes locally functionalized with a long-chain fatty acid. *Carbon*, 216:118533, 2024.

[89] Y. Maeda, Y. Konno, A. Nishino, M. Yamada, S. Okudaira, Y. Miyauchi, K. Matsuda, J. Matsui, M. Mitsuishi, and M. Suzuki. Sonochemical reaction to control the near-infrared photoluminescence properties of single-walled carbon nanotubes. *Nanoscale*, 12(11):6263–6270, 2020.

[90] Y. Zhang, N. Valley, A.H. Brozena, Y. Piao, X. Song, G.C. Schatz, and Y.H. Wang. Propagative

sidewall alkylcarboxylation that induces red-shifted near-ir photoluminescence in single-walled carbon nanotubes. *J. Phys. Chem. Lett.*, 4(5):826–830, 2013.

[91] Y. Maeda, S. Minami, Y. Takehana, J.-S. Dang, S. Aota, K. Matsuda, Y. Miyauchi, M. Yamada, M. Suzuki, R.-S. Zhao, X. Zhao, and S. Nagase. Tuning of the photoluminescence and up-conversion photoluminescence properties of single-walled carbon nanotubes by chemical functionalization. *Nanoscale*, 8(38):16916–16921, 2016.

[92] Y. Maeda, Y. Konno, M. Yamada, P. Zhao, X. Zhao, M. Ehara, and S. Nagase. Control of near infrared photoluminescence properties of single-walled carbon nanotubes by functionalization with dendrons. *Nanoscale*, 10:23012, 2018.

[93] Y. Maeda, K. Kuroda, H. Tambo, H. Murakoshi, Y. Konno, M. Yamada, P. Zhao, X. Zhao, S. Nagase, and M. Ehara. Influence of local strain caused by cycloaddition on the band gap control of functionalized single-walled carbon nanotubes. *RSC Adv.*, 9(25):13998–14003, 2019.

[94] Y. Maeda, Y. Suzuki, Y. Konno, P. Zhao, N. Kikuchi, M. Yamada, M. Mitsuishi, A.T.N. Dao, H. Kasai, and M. Ehara. Selective emergence of photoluminescence at telecommunication wavelengths from cyclic perfluoroalkylated carbon nanotubes. *Commun. Chem.*, 6:159, 2023.

[95] Y. Maeda, T. Kato, T. Hasegawa, M. Kako, T. Akasaka, J. Lu, and S. Nagase. Two-step alkylation of single-walled carbon nanotubes: Substituent effect on sidewall functionalization. *Org. Lett.*, 12(5):996–999, 2010.

[96] Y. Maeda, K. Saito, N. Akamatsu, Y. Chiba, S. Ohno, Y. Okui, M. Yamada, T. Hasegawa, M. Kako, and T. Akasaka. Analysis of functionalization degree of single-walled carbon nanotubes having various substituents. *J. Am. Chem. Soc.*, 134(43):18101–18108, 2012.

[97] Y. Maeda, Y. Takehana, M. Yamada, M. Suzuki, and T. Murakami. Control of the photoluminescence properties of single-walled carbon nanotubes by alkylation and subsequent thermal treatment. *Chem. Commun.*, 51(70):13462–13465, 2015.

[98] Y. Maeda, R. Morooka, P. Zhao, D. Uchida, Y. Konno, M. Yamada, and M. Ehara. Controlling near-infrared photoluminescence properties of single-walled carbon nanotubes by substituent effect in stepwise chemical functionalization. *J. Phys. Chem. C*, 127(5):2360–2370, 2023.

[99] S. Settele, F.J. Berger, S. Lindenthal, S. Zhao, A. Ali El Yumin, N.F. Zorn, A. Asyuda, M. Zharnikov, A. Högele, and J. Zaumseil. Synthetic control over the binding configuration of luminescent sp^3-defects in single-walled carbon nanotubes. *Nat. Commun.*, 12:2119, 2021.

[100] D. Just, R. Siedlecki, B. Podleśny, and D. Janas. Synchronous sorting and functionalization of single-walled carbon nanotubes using organic derivatives of hydrazine. *Adv. Optical Mater.*, 13(12):2402873, 2025.

[101] Y. Maeda, Y. Iguchi, P. Zhao, A. Suwa, Y. Taki, K. Kawada, M. Yamada, M. Ehara, and M. Kako. Switching photoluminescence wavelength of arylated single-walled carbon nanotubes by utilizing steric hindrance in reductive arylation. *Chem. - Eur. J.*, 31(13):e202404529, 2025.

[102] H. Onitsuka, T. Fujigaya, N. Nakashima, and T. Shiraki. Wavelength control of near-infrared photoluminescence of locally-functionalized single-walled carbon nanotubes through molecular recognition. *Chem. - Eur. J.*, 24(37):9393–9398, 2018.

[103] M. Kim, L. Adamska, N.F. Hartmann, H. Kwon, J. Liu, K.A. Velizhanin, Y. Piao, L.R. Powell,

S. Meany, S.K. Doorn, S. Tretiak, and Y. Wang. Fluorescent carbon nanotube defects manifest substantial vibrational reorganization. *J. Phys. Chem. C*, 120(20):11268–11276, 2016.

[104] T. Shiraki, T. Shiraishi, G. Juhász, and N. Nakashima. Emergence of new red-shifted carbon nanotube photoluminescence based on proximal doped-site design. *Sci. Rep.*, 6:28393, 2016.

[105] A. Saha, B.J. Gifford, X. He, G. Ao, M. Zheng, H. Kataura, H. Htoon, S. Kilina, S. Tretiak, and S.K. Doorn. Narrow-band single-photon emission through selective aryl functionalization of zigzag carbon nanotubes. *Nat. Chem.*, 10(11):1089–1095, 2018.

[106] F.J. Berger, J.A. de Sousa, S. Zhao, N.F. Zorn, A.A. El Yumin, A.Q. García, S. Settele, A. Högele, N. Crivillers, and J. Zaumseil. Interaction of luminescent defects in carbon nanotubes with covalently attached stable organic radicals. *ACS Nano*, 15(3):4327–4336, 2021.

[107] P. Wang, J. Fortner, H. Luo, J. Kłos, X. Wu, H. Qu, F. Chen, Y. Li, and Y.H. Wang. Quantum defects: What pairs with the aryl group when bonding to the sp^2 carbon lattice of single-wall carbon nanotubes? *J. Am. Chem. Soc.*, 144(29):13234–13241, 2022.

[108] C. Ma, X. Chen, S. V. Kurek, K. Li, Y. Zheng, R. He, Y. Piao, and Y. Wang. Stochastic formation of quantum defects in carbon nanotubes. *ACS Nano*, 17(9):20525–20533, 2023.

[109] T. Shiraishi, T. Shiraki, and N. Nakashima. Substituent effects on the redox states of locally functionalized single-walled carbon nanotubes revealed by in situ photoluminescence spectroelectrochemistry. *Nanoscale*, 9:16900–16907, 2017.

[110] F.L. Sebastian, F. Becker, Y. Yomogida, Y. Hosokawa, S. Settele, S. Lindenthal, K. Yanagi, and J. Zaumseil. Unified quantification of quantum defects in small-diameter single-walled carbon nanotubes by raman spectroscopy. *ACS Nano*, 17(21):21771–21781, 2023.

[111] L. Przypis, M. Krzywiecki, Y. Niidome, H. Aoki, T. Shiraki, and D. Janas. Enhancing near-infrared photoluminescence from single-walled carbon nanotubes by defect-engineering using benzoyl peroxide. *Sci. Rep.*, 10:19877, 2020.

[112] K. Nozaki and P.D. Bartlett. The kinetics of decomposition of benzoyl peroxide in solvents. i. *J. Am. Chem. Soc.*, 68(9):1686–1692, 1946.

[113] C.A. Barson and J.C. Bevington. Decomposition of benzoyl peroxide in dilute solutions. *J. Polym. Sci.*, 20(94):133–136, 1956.

[114] P.D. Bartlett and K. Nozaki. The decomposition of benzoyl peroxide in solvents. II. ethers, alcohols, phenols and amines. *J. Am. Chem. Soc.*, 69(10):2299–2306, 1947.

[115] Y. Maeda, Y. Takehana, J.-S. Dang, M. Suzuki, M. Yamada, and S. Nagase. Effect of substituents and initial degree of functionalization of alkylated single-walled carbon nanotubes on their thermal stability and photoluminescence properties. *Chem. - Eur. J.*, 23(8):1789–1794, 2017.

[116] C.G. Swain, W.H. Stockmayer, and J.T. Clarke. Effect of structure on the rate of spontaneous thermal decomposition of substituted benzoyl peroxides. *J. Am. Chem. Soc.*, 72(12):5426–5434, 1950.

[117] A.T. Blomquist and A.J. Buselli. The decomposition of sym-substituted benzoyl peroxides. *J. Am. Chem. Soc.*, 73(8):3883–3888, 1951.

[118] M. Pfohl, D. D. Tune, A. Graf, J. Zaumseil, R. Krupke, and B. S. Flavel. Fitting single-walled carbon nanotube optical spectra. *ACS Omega*, 2(3):1163–1171, 2017.

[119] S. R. Sanchez, S. M. Bachilo, Y. Kadria-Vili, C. W. Lin, and R. B. Weisman. (n,m)-specific

absorption cross sections of single-walled carbon nanotubes measured by variance spectroscopy. *Nano Lett.*, 16(11):6903–6909, 2016.

[120] S. K. Panigrahi and A. K. Mishra. Inner filter effect in fluorescence spectroscopy: As a problem and as a solution. *J. Photochem. and Photobiology C: Photochem. Rev.*, 41:100318, 2019.

[121] W. Yi, A. Malkovskiy, Q. H. Chu, A. P. Sokolov, M. Lebrón Colon, M. Meador, and Y. Pang. Wrapping of single-walled carbon nanotubes by a π-conjugated polymer: the role of polymer conformation-controlled size selectivity. *J. Phys. Chem. B*, 112(39):12263–12269, 2008.

[122] L. Ye and B. C. Thompson. p-Cymene: A sustainable solvent that is highly compatible with direct arylation polymerization (DArP). *ACS Macro Lett.*, 10(6):714–719, 2021.

[123] T. Lei, X. Chen, G. Pitner, H.-S. P. Wong, and Z. Bao. Removable and recyclable conjugated polymers for highly selective and high-yield dispersion and release of low-cost carbon nanotubes. *J. Am. Chem. Soc.*, 138(3):802–805, 2016.

[124] X. Yu, D. Liu, L. Kang, Y. Yang, X. Zhang, Q. Lv, S. Qiu, H. Jin, Q. Song, J. Zhang, and Q. Li. Recycling strategy for fabricating low-cost and high-performance carbon nanotube TFT devices. *ACS Appl. Mater. Interfaces*, 9(18):15719–15726, 2017.

[125] T. Li, H. Zhang, B. Liu, T. Ma, J. Lin, L. Xie, and D. Lu. Effect of solvent on the solution state of conjugated polymer P7DPF: Including single-chain to aggregated state structure formation, dynamic evolution, and related mechanisms. *Macromolecules*, 53(11):4264–4273, 2020.

[126] Y. Yang, D.J. Miller, and S.B. Hawthorne. Toluene solubility in water and organic partitioning from gasoline and diesel fuel into water at elevated temperatures and pressures. *J. Chem. Eng. Data*, 42(5):908–913, 1997.

[127] G.A. Russell. The effect of oxygen on the decomposition of α, α'-azodiisobutyronitrile and benzoyl peroxide in aromatic solvents. *J. Am. Chem. Soc.*, 78(5):1044–1046, 1956.

[128] M.G. Simic. Free radical mechanisms in autoxidation processes. *J. Chem. Educ.*, 58(2):125–130, 1981.

[129] S.C.W. Hook and B. Saville. The trapping of carbon radicals: The competition of oxygen and iodine for the 1,1-diphenylethyl radical. *J. Chem. Soc., Perkin Trans. 2*, 6:589–593, 1975.

[130] C.F.H. Tipper. 568. the effect of water on the decomposition of benzoyl peroxide. *J. Chem. Soc.*, 0:2966–2971, 1952.

[131] J.M. Cuerva, A.G. Campaña, J. Justicia, A. Rosales, J.L. Oller-López, R. Robles, D.J. Cárdenas, E. Buñuel, and J.E. Oltra. Water: the ideal hydrogen-atom source in free-radical chemistry mediated by Ti(III) and other single-electron-transfer metals? *Angew. Chem., Int. Ed.*, 45(33):5522–5526, 2006.

[132] V.T. Perchyonok. Organic radical reductions in water: Water as a hydrogen atom source. In *Streamlining Free Radical Green Chemistry*. RSC, 2011.

[133] G. Litwinienko, A.L.J. Beckwith, and K.U. Ingold. The frequently overlooked importance of solvent in free radical syntheses. *Chem. Soc. Rev.*, 40(5):2157–2163, 2011.

[134] T. Shiraki, Y. Niidome, F. Toshimitsu, T. Shiraishi, T. Shiga, B. Yu, and T. Fujigaya. Solvatochromism of near infrared photoluminescence from doped sites of locally functionalized single-walled carbon nanotubes. *Chem. Commun.*, 55(25):3662–3665, 2019.

[135] R.N. Chadha, J.S. Shukla, and G.S. Misra. Studies in chain-transfer. Part 2. Catalyzed polymerization of methyl methacrylate. *Trans. Faraday Soc.*, 53:240–246, 1957.

[136] R.C. Lamb and J.R. Sanderson. Organic peroxides. VIII. kinetics and free-radical efficiencies in the thermal decompositions of some mixed isobutyryl-substituted benzoyl peroxides. *J. Am. Chem. Soc.*, 91(18):5034–5038, 1969.

[137] M.E. Kurzu and M. Pellegrini. Electrophilic properties of benzoyloxy radicals. *J. Org. Chem.*, 35(4):990–992, 1970.

[138] J. Chateauneuf, J. Lusztyk, and K.U. Ingold. Spectroscopic and kinetic characteristics of aroyloxyl radicals. 2. Benzoyloxyl and ring-substituted aroyloxyl radicals. *J. Am. Chem. Soc.*, 110(9):2886–2893, 1988.

[139] Y.K. Syrkin and I.I. Moiseev. The mechanisms of some peroxide reactions. *Russ. Chem. Rev.*, 29(4):193–214, 1960.

[140] B. Yu, S. Naka, H. Aoki, K. Kato, D. Yamashita, S. Fujii, Y.K. Kato, T. Fujigaya, and T. Shiraki. Ortho-substituted aryldiazonium design for the defect configuration-controlled photoluminescent functionalization of chiral single-walled carbon nanotubes. *ACS Nano*, 16(12):21452–21461, 2022.

[141] B.M. Maciejewska, M. Jasiurkowska-Delaporte, A.I. Vasylenko, K.K. Kozioł, and S. Jurga. Experimental and theoretical studies on the mechanism for chemical oxidation of multiwalled carbon nanotubes. *RSC Adv.*, 4(55):28826–28831, 2014.

[142] L. Luer, S. Hoseinkhani, D. Polli, J. Crochet, T. Hertel, and G. Lanzani. Size and mobility of excitons in (6,5) carbon nanotubes. *Nat. Phys.*, 5(1):54–58, 2009.

[143] A.J. Siitonen, D.A. Tsyboulski, S.M. Bachilo, and R.B. Weisman. Dependence of exciton mobility on structure in single-walled carbon nanotubes. *J. Phys. Chem.*, 1(14):2189–2192, 2010.

[144] F.L. Sebastian, S. Settele, H. Li, B.S. Flavel, and J. Zaumseil. How to recognize clustering of luminescent defects in single-wall carbon nanotubes. *Nanoscale Horiz.*, 9(12):2286–2294, 2024.

[145] Z. Chen, W. Thiel, and A. Hirsch. Reactivity of the convex and concave surfaces of single-walled carbon nanotubes (SWCNTs) towards addition reactions: Dependence on the carbon-atom pyramidalization. *ChemPhysChem*, 4(1):93–97, 2003.

[146] Y. Li nad S. Osuna, M. Garcia-Borras, X. Qi, S. Liu, K.N. Houk, and Y. Lan. Reactivity of single-walled carbon nanotubes in the diels–alder cycloaddition reaction: distortion–interaction analysis along the reaction pathway. *Chem. - Eur. J.*, 22(36):12819–12824, 2016.

Research Achievements

Other published **research articles** not included in this work:

1. B. Podleśny, Ł. Czapura, P. Taborowska, L. Zhang, F. Yang and D. Janas, **A universal approach for extraction of single-walled carbon nanotubes of specific chirality using aqueous two-phase extraction.**, *Nano Res.*, 18(2):94907112. DOI: 10.26599/NR.2025.94907112.
2. A. Dzienia, D. Just, P. Taborowska, A. Mielańczyk, K.Z. Milowska, S. Yorozuya, S. Naka, T. Shiraki and D. Janas, **Mixed-Solvent Engineering as a Way around the Trade-Off between Yield and Purity of (7,3) Single-Walled Carbon Nanotubes Obtained Using Conjugated Polymer Extraction.**, *Small*, 19(46):2304211, 2023. DOI: 10.1002/smll.202304211.
3. P. Taborowska, D. Janas, **Seamless design of thermoelectric modules from single-walled carbon nanotubes**, *J. Mat. Chem. C*, 10:6818–6826, 2022. DOI: 10.1039/D2TC00821A.
4. P. Taborowska, G. Stando, M. Sahlman, M. Krzywiecki, M. Lundström and Dawid Janas, **Doping of carbon nanotubes by halogenated solvents.**, *Sci. Rep.*, 12:7004, 2022. DOI: 10.1038/s41598-022-11162-3.
5. P. Taborowska, T. Wasiak, M. Sahlman, M. Lundström and D. Janas, **Carbon Nanotube-Based Thermoelectric Modules Enhanced by ZnO Nanowires.**, *Materials*, 15(5):1924, 2022. DOI: 10.3390/ma15051924.
6. S. Lepak-Kuc, P. Taborowska, T.Q. Tran, H.M. Duong, T. Gizewski, M. Jakubowska, J. Patmore, A. Lekawa-Raus, **Washable, colored and textured, carbon nanotube textile yarns**, *Carbon*, 172:334–344, 2021. DOI: 10.1016/j.carbon.2020.10.045.
7. P. Taborowska, T. Giżewski, J. Patmore, D. Janczak, M. Jakubowska, A. Lekawa-Raus, **Spun Carbon Nanotube Fibres and Films as an Alternative to Printed Electronic Components**, *Materials*, 13(2):431, 2020. DOI: 10.3390/ma13020431.

Participation in **research projects**:

1. ENIGMA: dEciphering Nanochemistry by usInG cheMical modification of cArbon nanotubes for modern medicine 2020/39/D/ST5/00285.
2. Nanohybr1Ds: Hybrids composed of carbon nanotubes and metallic nanowires for harvesting energy from waste heat, LIDER/0001/L-8/16/NCBR/2017.
3. Carbon Nanomaterials for our Energy Future, LIDER/220/L-6/14/NCBiR/2015.

Patents:

1. D. Janas, P. Taborowska: **Method of manufacturing thermoelectric modules based on carbon nanotubes.**, Polish Patent: Pat.246940, 2025.
2. A. Dzienia, D. Just, P. Taborowska, D. Janas: **Method of selective isolation of semi-conducting single-walled carbon nanotubes.**, Polish Patent: Pat.246683, 2024.
3. A. Lekawa-Raus, S.K. Lepak-Kuc, P. Taborowska: **Method of manufacturing of conductive carbon nanotube based textile fibres.**, Polish Patent: Pat.236859, 2020.

Conferences:

1. 2025 E-MRS Fall Meeting, Warsaw, Poland. Poster: Modification of photoluminescent emission from single-walled carbon nanotubes through aryl peroxide chemistry.
2. IEEE NAP-2023, Bratislava, Slovakia. Poster: Environmentally-conscious and cost-beneficial selective extraction of single-walled carbon nanotubes by conjugated polymer extraction.
3. XLIV-th IEEE-SPIE Joint Symposium Wilga 2019, Wilga, Poland. Speech: Carbon nanotube fibers doped with iron via Fenton reaction.
4. UltraWire Workshop 2018, Cambridge, England.
5. Graphene Commercialisation 2018, Cranfield, England.

Internships:

1. Indian Institute of Technology Roorkee (India), Institute Instrumentation Centre. March 2023. Characterization of photoluminescent nanocarbon structures.
2. Cranfield University (England), Enhanced Composites and Structures Centre. July – September 2018. Electrospinned graphene composites, their electrical and mechanical properties.